Impact of inherent periodic structure on effective medium description of left-handed and related metamaterials

Th. Koschny,[1,2] P. Markoš,[1,3] E. N. Economou,[2,4] D. R. Smith,[5,6] D. C. Vier,[6] and C. M. Soukoulis[1,2,7]
[1]*Ames Laboratory and Department of Physics and Astronomy, Iowa State University, Ames, Iowa 50011, USA*
[2]*Institute of Electronic Structure and Laser, FORTH, 71110 Heraklion, Crete, Greece*
[3]*Institute of Physics, Slovak Academy of Sciences, 845 11 Bratislava, Slovakia*
[4]*Department of Physics, University of Crete, 71110 Heraklion, Crete, Greece*
[5]*Department of Electrical and Computer Engineering, Duke University, Durham, North Carolina 27708, USA*
[6]*Department of Physics, University of California, San Diego, La Jolla, California 92093, USA*
[7]*Department of Materials Science and Technology, University of Crete, 71110 Heraklion, Crete, Greece*
(Received 2 November 2004; revised manuscript received 24 February 2005; published 8 June 2005)

We study the frequency dependence of the effective electromagnetic parameters of left-handed and related metamaterials of the split ring resonator and wire type. We show that the reduced translational symmetry (periodic structure) inherent to these metamaterials influences their effective electromagnetic response. To anticipate this periodicity, we formulate a periodic effective medium model which enables us to distinguish the resonant behavior of electromagnetic parameters from effects of the periodicity of the structure. We use this model for the analysis of numerical data for the transmission and reflection of periodic arrays of split ring resonators, thin metallic wires, cut wires, as well as the left-handed structures. The present method enables us to identify the origin of the previously observed resonance-antiresonance coupling as well as the occurrence of negative imaginary parts in the effective permittivities and permeabilities of those materials. Our analysis shows that the periodicity of the structure can be neglected only for the wavelength of the electromagnetic wave larger than 30 space periods of the investigated structure.

DOI: 10.1103/PhysRevB.71.245105 PACS number(s): 41.20.Jb, 42.25.Bs, 42.70.Qs, 73.20.Mf

I. INTRODUCTION

Recent progress in studies of left-handed metamaterials[1] (LHMs) confirmed that the fabrication of structures with negative *effective* permittivity and permeability, and their application in technical praxis is possible. The most promising structures are based on the combination of periodic arrays of metallic split ring resonators (SRRs) and thin metallic wires, a design proposed theoretically by Pendry *et al.*[2–4] and experimentally verified by Smith *et al.*[5–7]

It is assumed that in a well defined frequency interval both effective permittivity and permeability of LHM are simultaneously negative. Consequently, also the refractive index is negative.[8] This theoretical prediction was supported experimentally by measurements of the transmission of the electromagnetic (EM) wave through the LHM: A transmission peak was observed in the frequency region where the LH band is expected.[5,6] Negativeness of the index of refraction was verified experimentally by the Snell's law experiment[7] and confirmed later by other experiments.[9,10] Numerical simulations were performed which also observed a transmission peak in the resonant frequency interval.[11–13] Effective electromagnetic parameters were calculated[14] by comparison of numerically obtained transmission and reflection amplitudes of the LHM with theoretical formulas for a *homogeneous* slab. The obtained results confirmed that the refractive index of the LHM is indeed negative in the resonant frequency interval. Moreover, the obtained frequency dependence of the effective permittivity and permeability also agreed qualitatively with theoretical predictions. In particular, the effective magnetic permeability shows a resonant behavior

$$\mu(\omega) = 1 - \frac{\omega_{mp}^2 - \omega_m^2}{\omega^2 - \omega_m^2 + i\gamma\omega}, \tag{1}$$

typical for lattice of SRR (Ref. 4) in the vicinity of the magnetic resonance frequency ω_m. The effective permittivity is determined by the electric response of the array of thin wires[3,15–17]

$$\varepsilon(\omega) = 1 - \frac{\omega_p^2}{\omega^2 + i\gamma\omega} \tag{2}$$

and is negative if the frequency is smaller than the plasma frequency ω_p. Transmission data, obtained using either the transfer matrix method[12] or commercial software[18] was analyzed to find the dependence of the resonance frequency ω_m on the structural parameters of the SRR and on the design of the unit cell of the LHM structure.

Further progress in numerical methods brought more accurate data and strong evidence that the effective parameters of the LHM differ considerably from the theoretical prediction (1) and (2). Although the main properties—resonant behavior of the magnetic permeability at ω_m and negativeness of the effective permittivity—are clearly visible in the data, the effective medium picture is spoiled by partially very significant anomalies.

Resonance-antiresonance coupling. We expect the electric and magnetic response of the discussed metamaterials to be independent from each other. However, whenever there is a resonance in Re μ, we simultaneously observe an antiresonant behavior in Re ε (Refs. 14 and 19–22) and vice versa.[23] The antiresonant structures in the real part are accompanied by a negative imaginary part.[20,23]

Misshapen, truncated resonances. The divergence in Re n appears to be cutoff at the edges of the first Brillouin zone and, in particular, the negative regions of the magnetic resonance in μ and cut-wire resonance in ε do not return from large negative real part but seem to saturate in a rather shallow behavior. The corresponding absorption peak in the imaginary parts is misshapen and highly asymmetric too.[23]

Discrepancy between n and z about the positions of the resonances. We expect the peaks (or zeros) in the index of refraction and the impedance to appear exactly at the resonance frequency. From the simulations, however, we find different frequencies from n and z, respectively. This leads, for instance, to an "internal structure" of the magnetic resonance as shown in Figs. 5 and 6. This structure cannot easily be explained within the assumed effective medium picture.[23]

Additional spectral structures. Apart from structures around the anticipated contributions of the metamaterial's constituents, we observe a lot of additional structure, especially at higher frequency, which cannot be accounted for.

The above described observation, especially the negativeness of the imaginary part of effective permittivity or permeability, raised objections[24,25] of other groups. Efros[25] argued that the LHM cannot be approximated by a homogeneous system because of the periodicity of the metamaterial.[17,26,27]

In this paper, we show that the observed artifacts in the homogeneous effective approximation are quite generic. They are given by the periodic structure of the investigated metamaterials. The periodic structure becomes important when the wavelength of the electromagnetic wave is comparable with the lattice structure of the material.[23] We proposed a more general description of the LHM, based on the concept of a periodic effective medium (PEM). This method enables us to distinguish between the resonant frequency dependence corresponding to Eq. (1) and effects of the periodicity of the structure. We apply the PEM method for the analysis of numerical data obtained by the transfer matrix method (TMM).

The paper is organized as follows. In Sec. II we first explain basic ideas of the homogeneous effective medium (HEM). Special attention is given to the correction of the phase of the EM wave at the interfaces, which is crucial for any retrieval procedure.

In Sec. III we define and analyze one dimensional periodic structures. The analyzed medium consists of thin slabs of homogeneous LH material separated by slabs of vacuum. We show that the approximation of such periodic medium by a homogeneous one give us effective parameters ε and μ which possess unusual frequency dependences, similar to those observed when we approximate metamaterials by a homogeneous medium. This proves that the periodicity of metamaterial must be taken into consideration in the analysis of the effective parameters.

The periodic effective medium is analyzed in two different formulations: continuous (Sec. III A) and lattice (Sec. III B). The latter is more relevant for the analysis of numerical data since all known numerical algorithms use spacial discretization.

In Sec. IV we analyze transmission data, observed from numerical simulations of periodic lattices of SRR, LHM, and cut wires. We map these structures to periodic effective media which consist of homogeneous slabs separated by vacuum. In this formulation, ε and μ of the homogeneous slabs are free from any modifications of the resonant behavior. To show the role of the periodicity of the metamaterials more clearly, we also analyzed a lattice of SRR in which we filled the gaps of the SRR by a dielectric with very strong dielectric permittivity. This decreases the magnetic resonant frequency so that the wavelength of the incident EM wave is 25 times larger than the lattice period. We show that effective parameters again do not possess any deviations from resonant formula (1).

A discussion of the applicability of various proposed models to the analysis of transmission data is given in Sec. V. We discuss how the periodicity and anisotropy of the structure influence the transmission amplitudes and, subsequently, the effective parameters of the metamaterials. Final conclusions are given in Sec. VI.

II. HOMOGENEOUS EFFECTIVE MEDIUM

For the one-dimensional plain wave scattering problem at a homogeneous finite slab it is straightforward to obtain the scattering formulas. For the transfer matrices $\mathbf{T}_0$ for a single slice of vacuum and $\mathbf{T}_{\text{slab}}$ for a single slice of homogeneous material with the thickness d we find in wave representation[44]

$$\mathbf{T}_0(d) = \begin{pmatrix} e^{ikd} & 0 \\ 0 & e^{-ikd} \end{pmatrix}, \quad \mathbf{T}_{\text{slab}}(d) = \begin{pmatrix} \alpha(d) & \beta(-d) \\ \beta(d) & \alpha(-d) \end{pmatrix}$$

with the elements

$$\alpha(d) = \cos(qd) + \frac{i}{2}\left(z + \frac{1}{z}\right)\sin(qd), \tag{3}$$

$$\beta(d) = \frac{i}{2}\left(z - \frac{1}{z}\right)\sin(qd). \tag{4}$$

In the continuum formulation and for normal incidence the momentum q inside the slab is related to the momentum k in the vacuum by the index of refraction $n(k)=q/k$, the impedance z is defined by $z=\mu(\omega)k/q=q/[\varepsilon(\omega)k]$ for the TE and TM mode, respectively. Here, $\mu(\omega)$ and $\varepsilon(\omega)$ denote the frequency-dependent complex permeability and permittivity of the homogeneous medium. On the lattice, i.e., when we are going to compare with TMM simulation results, we have to take the modified dispersion relations $2-2\cos(k)-\omega^2=0$ in the vacuum and $2-2\cos(q)-\mu(\omega)\varepsilon(\omega)\omega^2=0$ inside the slab into account. Then we have a modified $q=\text{acos}[1-\mu\varepsilon(1-\cos k)]$ which gets noticeable at higher frequencies. Using the interrelation between the transfer matrix and the scattering matrix which defines the transmission ($t_{\pm}$) and reflection ($r_{\mp}$) amplitudes

$$\mathbf{S} = \begin{pmatrix} t_+ & r_+ \\ r_- & t_- \end{pmatrix}, \quad \mathbf{T} = \begin{pmatrix} t_+ - r_+ t_-^{-1} r_- & r_+ t_-^{-1} \\ -t_-^{-1} r_- & t_-^{-1} \end{pmatrix}, \tag{5}$$

we can calculate the transmission and reflection amplitudes for a sample composed of a left vacuum slice of length a, followed by N homogeneous unit cells of length L in propa-

gation direction, and terminated by a right vacuum slice of length b,

$$t_- = \frac{e^{-ikNL}}{\alpha(-d)e^{-ik(a+b)}}, \tag{6}$$

$$r_+ = e^{-ikNL}\beta(-d)e^{-ik(a-b)}t_-. \tag{7}$$

In order to relate to the simulated scattering amplitudes computed numerically by the TMM by decomposition of the EM waves in the vacuum right of the sample with respect to the vacuum wave base left of the sample, it is convenient to introduce the normalized scattering amplitudes T and R which, after N unit cells, take the form

$$T = t_- e^{ikNL} = \alpha^{-1}(-d)e^{ik(a+b)}, \tag{8}$$

$$R = \beta(-d)e^{-ik(a-b)}T. \tag{9}$$

In the continuum the scattering amplitudes of the homogeneous slab are typically defined from interface to interface of the sample, i.e., assuming $a=b=0$. In the numerical simulation this is not possible because of the lattice: we always have to make $1/2$ vacuum-transfer-matrix step from the last left vacuum slice into the sample and another $1/2$ vacuum-transfer-matrix step out of the sample onto the first right vacuum slice. Therefore, the TMM scattering amplitudes $T^{(\mathrm{TMM})}$ and $R^{(\mathrm{TMM})}$ are related to the normalized T and R involving an additional vacuum-phase compensation $T=e^{-ik}T^{(\mathrm{TMM})}$ and $R=e^{+ik}R^{(\mathrm{TMM})}$.

Now we can resolve the above scattering formulas with given amplitudes T and R obtained from the simulation (or measurement) of a metamaterial with respect to the material parameters impedance $z(\omega)$ and index of refraction $n(\omega)$. If the solutions are (virtually) independent on the length of the sample those parameters define the homogeneous effective medium (HEM) representation (or approximation) of the respective metamaterial. Then we have[14]

$$z_{\mathrm{eff}}(\omega) = \pm\sqrt{\frac{(1+R)^2 - T^2}{(1-R)^2 - T^2}}, \tag{10}$$

$$n_{\mathrm{eff}}(\omega) = \pm\frac{1}{kL}\arccos\left(\frac{1-R^2+T^2}{2T}\right) + \frac{2\pi}{kL}m, \tag{11}$$

with $m \in \mathbb{Z}$. Note that we obtain z_{eff} and n_{eff} from the scattering amplitudes only up to a common sign and the real part of the effective index of refraction, $\mathrm{Re}\, n_{\mathrm{eff}}$ only as a residue class. The former issue can be resolved by imposing additional physical requirements, for instance $\mathrm{Re}\, z \geqslant 0$ (causality). The problem of the residue class for $\mathrm{Re}\, n_{\mathrm{eff}}$ can be addressed by considering different length $\{L_i\}$, $i \in I \subset \mathbb{Z}$. Then we obtain a system of linear congruences, the solution of which—if any—is a reduced residue class modulo $2\pi/(k\,\mathrm{gcd}\{L_i\})$ given by the greatest common divisor of the lengths L_i. Since due to the inherent periodic structure of real metamaterials in simulations and experiments the lengths of the sample can only be integral multiples of the unit cell's length, the minimum possible ambiguity for $\mathrm{Re}\, n_{\mathrm{eff}}$ will be a residue class modulo $2\pi/(kL)$ where L is the length of a single unit cell. For physical reasons we can assume a smooth frequency dependence between resonances which enables us to obtain $\mathrm{Re}\, n_{\mathrm{eff}}(\omega)$ as the corresponding residue class of piecewise continuous functions. The correct branch then has to be chosen exploiting additional physical information or assumptions of the model such as the behavior of $n_{\mathrm{eff}}(\omega)$ at the plasma frequency, in resonance induced transmission gaps and periodicity induced band gaps (discussed later). For known $n_{\mathrm{eff}}(\omega)$ and $z_{\mathrm{eff}}(\omega)$ the effective permeability μ and permittivity ε can be defined as

$$\mu_{\mathrm{eff}}(\omega) = n_{\mathrm{eff}}(\omega)z_{\mathrm{eff}}(\omega), \tag{12}$$

$$\varepsilon_{\mathrm{eff}}(\omega) = n_{\mathrm{eff}}(\omega)/z_{\mathrm{eff}}(\omega), \tag{13}$$

respectively.

Results for the effective parameters of the HEM approximation of simulated metamaterials such as arrays of SRR or cut wires, LHMs, and even multigap SRRs have been published by several authors.[7,13,14,19,22,23,28] They all expose details which are in conflict with the simple effective medium behavior in terms of a resonant $\mu(\omega)$ and a plasmonic $\varepsilon(\omega)$, originally proposed by Pendry, even under the assumption of an additional electric response of the SRR. Typical examples are also shown in Figs. 5, 6, 9, and 10. All results show resonance/anti-resonance coupling in $\mu_{\mathrm{eff}}(\omega)$ and $\varepsilon_{\mathrm{eff}}(\omega)$ accompanied by negative imaginary parts, apparently different resonance frequencies for n_{eff} and z_{eff}, the cutoff of the expected resonant positive (SRR) or negative (LHM) index of refraction, a misshapen, strongly asymmetric anticipated magnetic resonance in μ for the SRR and LHM or electric resonance in ε for the cut wire, and finally a lot of unexplained additional structure (erratic stop bands and pass bands) at higher frequency.

Our extensive numerical simulations suggested that common cause for all these problems has to be sought in the inherent periodicity, always present in the artificial metamaterials as they are composed of repetitions of a single unit cell. To prove that the behavior is generic and really independent on the details of the unit cell, and that we can reproduce each of the effects above purely as a consequence of periodicity in the propagation direction, we investigated the most simple model for an effective medium with a nontrivial periodicity.

III. PERIODIC EFFECTIVE MEDIUM

To study the impact of the periodicity, or more precise the reduced translational symmetry of the sample in propagation direction, we consider a sample composed of a repetition of the unit cell shown in Fig. 1, finite in direction of propagation and infinite perpendicular to it. The unit cell consists of a thin homogeneous core of thickness d characterized by arbitrary $\mu(\omega)$ and $\varepsilon(\omega)$, sandwiched by two slabs of vacuum with thickness a and b which break translational invariance. L is the length of one unit cell, N the number of unit cells in propagation direction. To make a connection to our metamaterials we choose a simple Lorentz-type resonant form of $\mu(\omega)$ and/or $\varepsilon(\omega)$ to represent the magnetic and cut-wire

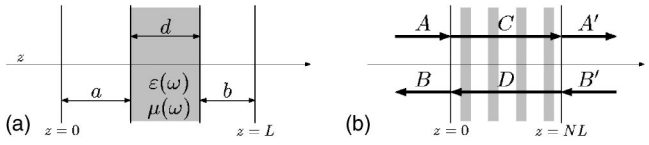

FIG. 1. The layout of the single unit cell (a) and of a finite slab of the model periodic medium are shown. The shaded regions indicate the homogeneous core of the width d which is characterized by the chosen appropriately model functions $\mu(\omega)$ and $\varepsilon(\omega)$, sandwiched by two vacuum slabs. L is the length of a single unit cell and N the number of unit cells in the slab in propagations direction. Periodic boundary conditions apply in the directions perpendicular to the propagation direction z.

response of the SRR. To model the LHM we would add a plasmonic term in $\varepsilon(\omega)$ to account for the response of the continuous wires. Now we can calculate the scattering amplitudes for this model and subject them to the HEM inversion discussed in the previous section. The description (or approximation) of the scattering amplitudes for a given metamaterial in terms of the effective parameters of such a periodic medium as defined in Fig. 1 will be denoted a "periodic effective medium" (PEM).

The following results will show that this periodic medium can expose all the problematic effect discussed above. In a subsequent section we shall then demonstrate that this also applies to the simulated real metamaterial. Their effective behavior can be decomposed into a "well-behaving" effective response of the resonances and a contribution of periodic structure described by the PEM.

A. Continuum formulation

With the transfer matrices $\mathbf{T}_0$ and $\mathbf{T}_{\text{slab}}$ introduced above, we can express the total transfer matrix of a finite slab of the periodic effective medium defined in Fig. 1 in the form

$$\begin{pmatrix} A' \\ B' \end{pmatrix} = \mathbf{T}_0^{-1}(NL)[\mathbf{T}_0(b)\mathbf{T}_{\text{slab}}(d)\mathbf{T}_0(a)]^N \begin{pmatrix} A \\ B \end{pmatrix}.$$

As expected from the z-inversion symmetry both transfer matrices $\mathbf{T}_0$ and $\mathbf{T}_{\text{slab}}$ are unimodular, obviously is $\det \mathbf{T}_0 = 1$ and a short calculation yields $\det \mathbf{T}_{\text{slab}} = \alpha(d)\alpha(-d) + \beta^2(d) = 1$. Therefore we can easily calculate the Nth power of the unimodular 2×2 matrix above by diagonalizing it and computing the Nth power of its eigenvalues.[30] Using the interrelation between the transfer matrix and the scattering matrix, we obtain the transmission and reflection amplitudes corresponding to those computed numerically by the TMM

$$t_- = \frac{e^{-ikNL}}{\alpha(-d)e^{-ik(a+b)}U_{N-1}(p) - U_{N-2}(p)}, \tag{14}$$

$$r_+ = e^{-ikNL}\beta(-d)e^{-ik(a-b)}U_{N-1}(p)t_-. \tag{15}$$

Here, the $U_N = U_N(p)$ are the Chebyshev polynomials of the second kind, $U_n(z) = \sin[(n+1)\arccos z]/(1-z^2)^{1/2}$, taken at the argument

$$p = \cos(qd)\cos[k(L-d)] - \frac{1}{2}\left(z + \frac{1}{z}\right)\sin(qd)\sin[k(L-d)]. \tag{16}$$

The wave vector $q = n(\omega)k$ and the impedance $z(\omega)$ refer to the homogeneous core of the unit cell. For the normalized scattering amplitudes T and R after N unit cells we find

$$T = [\alpha(-d)e^{-ik(a+b)}U_{N-1}(p) - U_{N-2}(p)]^{-1}, \tag{17}$$

$$R = \beta(-d)e^{-ik(a-b)}U_{N-1}(p)T. \tag{18}$$

Now we shall discuss what happens if we try to approximate the explicitly periodic medium discussed above by a homogeneous effective medium. This basically corresponds to our previous attempts to describe the periodic metamaterials by an homogeneous effective medium. We have two options: First, we could simply consider the analytic scattering amplitudes (17) and (18) derived above to be those of a homogeneous system and try to solve for effective material parameters $\varepsilon_{\text{eff}}(N,\omega)$ and $\mu_{\text{eff}}(N,\omega)$. This has the advantage that the approximation can deal with a possible residual length dependence of the approximate homogeneous medium, leaving an explicit possibility to assess the quality of the approximation. The disadvantage is that we have to handle the rather complicated structure of the formulas arising from the Chebyshev polynomials. The second approach is to assume that an exact correspondence of the periodic effective medium to an homogeneous effective medium exists. This assumption is supported by the length independence (after appropriate phase compensation) of the conventionally inverted simulation data. If there is such a homogeneous effective medium we can write the transfer matrix of the periodic medium in terms of the transfer matrix for the homogeneous slab

$$\mathbf{T}_0^{-1}(NL)[\mathbf{T}_0(b)\mathbf{T}_{\text{slab}}(d)\mathbf{T}_0(a)]^N = \mathbf{T}_0^{-1}(NL)\,{}^{(\text{eff})}\mathbf{T}_{\text{slab}}(NL), \tag{19}$$

which implies in particular for a system length of only a single unit cell

$$\mathbf{T}_0(b)\mathbf{T}_{\text{slab}}(d)\mathbf{T}_0(a) = {}^{(\text{eff})}\mathbf{T}_{\text{slab}}(L). \tag{20}$$

Since for a homogeneous slab the identity $\mathbf{T}_{\text{slab}}^N(L) = \mathbf{T}_{\text{slab}}(NL)$ holds, finding a ${}^{(\text{eff})}\mathbf{T}_{\text{slab}}(L)$ that satisfies Eq. (20) in turn implies length independence of the homogeneous effective medium description. Note that $\mathbf{T}_{\text{slab}}(d)$ has only two independent elements, because $\beta(d) = -\beta(-d)$ is antisymmetric and the determinant $\alpha(d)\alpha(-d) + \beta^2(d) = 1$ is fixed, such that we can calculate the matrix elements $\alpha(d) = [1-\beta^2(-d)]/\alpha(-d)$ and $\beta(d) = -\beta(-d)$ from $\alpha(-d)$, $\beta(-d)$. The assumption (20) imposes a restriction on the boundaries of the periodic medium in propagation direction. The off-diagonal elements of $\mathbf{T}_{\text{slab}}$ are antisymmetric but on the left side of Eq. (20) this symmetry is broken by the phase factors $e^{ik(a-b)}$ and $e^{-ik(a-b)}$ introduced in the off-diagonal elements by the two vacuum slabs. As a consequence the description as a homogeneous medium is only possible for $a-b=0$. In addition to choosing a symmetric unit cell in the first place

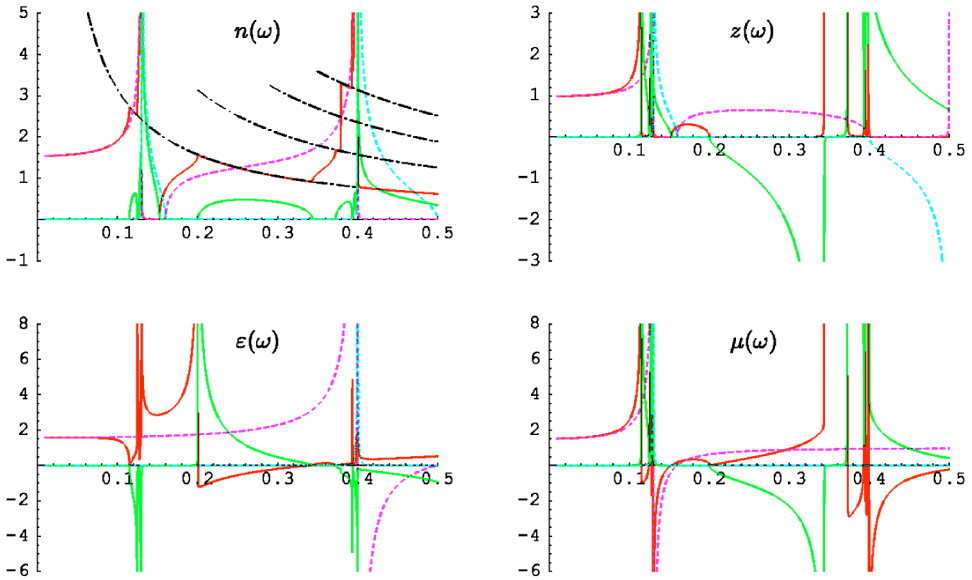

FIG. 2. (Color online.) The HEM inversion [Eqs. (24) and (25)] of the analytic continuum PEM scattering amplitudes [Eqs. (17) and (18)] for model SRR-type material parameters $\omega_m=0.13$, $\omega_{mp}=0.16$ for the magnetic and $\omega_e=0.4$, $\omega_{ep}=0.5$ for the electric response and $\gamma=10^{-4}$ [see Eqs. (29) and (30)]. The homogeneous core located in the middle of the unit cell was $d=L/10$ thick. The retrieved real (red, purple) and imaginary (green, turquoise) parts of effective parameters are shown as a function of frequency ω. The dashed lines show the real (purple) and imaginary (turquoise) parts of the anticipated homogeneous parameters [Eqs. (29) and (30)] and corresponding index of refraction and impedance. The dash-dotted black lines in Re n_{eff} indicate the upper edge of the Brillouin zone, $n_{\text{edge}}=k_{\text{edge}}/k=m\pi/(kL)$.

we may alternatively compensate the factor $e^{-ik(a-b)}$ in the reflection amplitude R [which works simultaneously for all lengths, see Eq. (18)], effectively redefining the boundaries of the system such that the slab is centered in the unit cells. In terms of the (normalized) scattering amplitudes T and R, for the single unit cell we then have the conditions

$$\alpha^{-1}(-d)e^{ik(L-d)} = T = \alpha_{\text{eff}}^{-1}(-L), \tag{21}$$

$$\beta(-d)T = R = \beta_{\text{eff}}(-L)T. \tag{22}$$

We already know how to invert the right side of these equations, this is just what we did in the retrieval procedure for the HEM in the previous section. Defining renormalized scattering amplitudes $T'=Te^{-ik(L-d)}$ and $R'=Re^{-ik(L-d)}$, we could apply the same procedure to the left side. Note that the possibility that we can always solve T and R for $\varepsilon_{\text{eff}}(\omega)$ and $\mu_{\text{eff}}(\omega)$ guarantees a solution of Eq. (20). In other words, there is always an exact, length-independent description of the periodic effective medium as a homogeneous effective medium characterized by $\varepsilon_{\text{eff}}(\omega)$ and $\mu_{\text{eff}}(\omega)$. There is no freedom to chose the boundaries of the homogeneous medium relative to the periodic medium. As shown above, we get the full information about the homogeneous effective medium which describes a given periodic effective medium characterized by $n(k)$,$z(k)$ and the geometry d,L already from the first unit cell. Inserting the renormalized transmission and reflection amplitudes (21) and (22) for a single unit cell into the inverted scattering formulas above we obtain

$$\cos[n_{\text{eff}}(k)kL] = \cos(nkd)\cos[k(L-d)] - \frac{1}{2}\left(z+\frac{1}{z}\right)\sin(nkd)\sin[k(L-d)], \tag{23}$$

where $n(k)$ and $z(k)$ are the parameters of the material slab in the middle of the unit cell of the periodic effective medium. With the p defined in Eq. (16) and $q=n(k)k$ we can write

$$n_{\text{eff}}(k) = \pm\frac{1}{kL}\arccos[p(n,z;k)] + \frac{2\pi}{kL}m \tag{24}$$

with $m\in\mathbb{Z}$. The problem with the signs of n_{eff} and z_{eff}, as well as with the ambiguity of Re n_{eff} is similar, and can be resolved the same way as for the case of the homogeneous slab discussed above. Analogously we can express the impedance z_{eff} of the effective homogeneous medium in terms of the n and z of the homogeneous core as

$$z_{\text{eff}}(k) = \pm\sqrt{\frac{2p^+ + (z-1/z)\sin(qd)}{2p^+ - (z-1/z)\sin(qd)}}, \tag{25}$$

where $q=n(k)k$ and

$$p^+ = \cos(qd)\sin[k(L-d)] + \frac{1}{2}\left(z+\frac{1}{z}\right)\sin(qd)\cos[k(L-d)]. \tag{26}$$

The parameters of an effective homogeneous medium describing the periodic material from Fig. 1, which have been obtained from the formulas (24) and (25), are shown in Fig. 2 for a concrete example of SRR-type $\mu(\omega)$ and $\varepsilon(\omega)$. For the homogeneous core in the middle of the unit cell we have chosen

$$\varepsilon(k) = 1 + (L/d)[\varepsilon_H(k) - 1], \tag{27}$$

$$\mu(k) = 1 + (L/d)[\mu_H(k) - 1] \tag{28}$$

with model functions

$$\mu_H(\omega) = 1 - \frac{\omega_{mp}^2 - \omega_m^2}{\omega^2 - \omega_m^2 + i\gamma\omega} \tag{29}$$

and

$$\varepsilon_H(\omega) = 1 - \frac{\omega_{ep}^2 - \omega_e^2}{\omega^2 - \omega_e^2 + i\gamma\omega} \tag{30}$$

to emulate the anticipated magnetic and electric[29] resonances of the SRR. For a LHM-type behavior we have to add the plasmonic response of the continuous wire in the permittivity

$$\varepsilon_H(\omega) = 1 - \frac{\omega_p^2}{\omega^2 + i\gamma\omega} - \frac{\omega_{ep}^2 - \omega_e^2}{\omega^2 - \omega_e^2 + i\gamma\omega}. \tag{31}$$

According to a simple effective medium picture, we would expect that we can approximate a homogeneous unit cell characterized by $\mu_H(\omega)$ and $\varepsilon_H(\omega)$ by concentration the magnetic and electric polarizations into the homogeneous core of the periodic medium. Figure 2 shows the actual effective impedance $z_{\text{eff}}(\omega)$ and index of refraction $n_{\text{eff}}(\omega)$ obtained via the HEM inversion of the periodic medium. Comparing with the expected effective medium behavior (dashed lines) we clearly see the typical anomalies in the shape and positions of the resonances, the same qualitative behavior as observed for real SRR metamaterials in the literature and our own previous work. The effective parameters of the HEM approximation of our periodic medium model show the resonance-antiresonance coupling in $\mu_{\text{eff}}(\omega)$ and $\varepsilon_{\text{eff}}(\omega)$ together with the negative imaginary part $\text{Im}\,\mu_{\text{eff}}(\omega) < 0$ around the magnetic resonance frequency ω_m, and also a very involved behavior close to the cut-wire resonance ω_e. The effective index of refraction is cut off at the edge of the Brillouin zone which corresponds to the appearance of additional band gaps origination from the periodicity rather than from the underlying material properties. The qualitative behavior presented in Fig. 2 is generic for a wide range of parameters $\omega_m, \omega_{mp}, \omega_e, \ldots$, of the resonances and L,d of the geometry. If the periodic medium model is used with only the electric resonance or with an additional plasmonic term in $\varepsilon(\omega)$, it qualitatively reproduces the observed deviations from the expected plain effective medium behavior published for the array of cut wires and the LHM, respectively.

Although the curves show most of the discussed abnormalities in the HEM description of the SRR, the analytic description matches the simulation and inversion results for the real metamaterial present in literature not in all aspects. Clearly, there are problems very close to the resonance frequencies. Instead of the divergence in the effective index of refraction n_{eff} being virtually cut off at the upper edge of the first Brillouin zone as observed in the simulations of the actual SRR metamaterial, the analytic description produces a series of consecutive band gaps at the boundaries of the first and higher Brillouin zones and a lot of structure in the imaginary part of n_{eff}. The same holds for the analytic description applied to the periodic effective medium model of the LHM (not shown). Here, we particularly miss the cutoff at the bottom of the negative n_{eff} region. In either case the underlying lattice in the simulation starts to become visible. Since the lattice has a finite lattice constant it cannot support arbitrarily large momenta, such that we expect additional effects if the continuum momentum q reaches the order of π/a_{lattice}. In order to understand also the details of the retrieved HEM parameters in our simulation of real SRR and LHM metamaterials we have to take the discretization lattice of the employed TMM into consideration. To see the modification of the continuum results by the discretization lattice we have to derive the scattering formulas for the periodic medium model on the lattice.

B. Lattice formulation

We follow the TMM introduced for the Maxwell equations by Pendry[31–34] in the formulation described by Markoš and Soukoulis.[12] The electric and magnetic field, together with the spatially dependent material relative constants $\mu_{\text{rel}}(\mathbf{r})$ and $\varepsilon_{\text{rel}}(\mathbf{r})$ which define the metamaterial, are discretized on the bonds of mutually dual lattices $\{\mathbf{m}\}$ and $\{\tilde{\mathbf{m}}\}$. With the renormalized material constants $\varepsilon_i(\mathbf{m}) = i\omega\varepsilon_0\varepsilon_{\text{rel}}(\mathbf{m} + \mathbf{e}_i/2)$ and $\mu_i(\mathbf{m}) = i\omega\mu_0\mu_{\text{rel}}(\tilde{\mathbf{m}} - \tilde{\mathbf{e}}_i/2)$, used throughout this section, we can write the transfer matrix equations for a stratification in the z direction for the two independent components $i \in \{x,y\}$ of the electromagnetic field. Using (quasi)periodic boundary conditions in the $\perp z$ plane we can introduce a Fourier representation of the fields with respect to this plane defining an in-plane momentum $\mathbf{q}$. To derive a scattering formula corresponding to the continuum case considered in the previous section we restrict ourself to the most simple case of normal incidence, i.e., zero in-plane momentum $\mathbf{q} = 0$. Then the transfer matrix for normal incidence takes the form

$$\begin{pmatrix} \mathbf{E} \\ \mathbf{H} \end{pmatrix}_{m_z+1} = \begin{pmatrix} 1 & \mathbf{A}(m_z) \\ \mathbf{B}(m_z+1) & 1 + \mathbf{B}(m_z+1)\mathbf{A}(m_z) \end{pmatrix} \begin{pmatrix} \mathbf{E} \\ \mathbf{H} \end{pmatrix}_{m_z}. \tag{32}$$

The generally $\mathbf{q}$-dependent matrices $\mathbf{A}$ and $\mathbf{B}$ reduce to a simple off-diagonal form, with the product $\mathbf{B}(m_z+1)\mathbf{A}(m_z)$ diagonal,

$$\mathbf{A}(m_z) = \begin{pmatrix} 0 & \mu_y(m_z) \\ -\mu_x(m_z) & 0 \end{pmatrix}, \tag{33}$$

$$\mathbf{B}(m_z) = \begin{pmatrix} 0 & -\varepsilon_y(m_z) \\ \varepsilon_x(m_z) & 0 \end{pmatrix}, \tag{34}$$

such that the transfer matrix (32) factorizes, reordering the electromagnetic field vector in the form $(E_x, H_y, E_y, -H_x)^T$, into a twofold degenerated block-diagonal structure

$$\begin{pmatrix} E_x & E_y \\ H_y & -H_x \end{pmatrix}_{m_z+1} = \begin{pmatrix} 1 & \mu_y(m_z) \\ \varepsilon_x(m_z+1) & 1+\varepsilon_x(m_z+1)\mu_y(m_z) \end{pmatrix} \times \begin{pmatrix} E_x & E_y \\ H_y & -H_x \end{pmatrix}_{m_z}. \tag{35}$$

Without loss of generality we can restrict ourself to consider just the first polarization. We denote the single-polarization transfer matrix for the $\mathbf{q}=0$ modes in the last equation $T(m_z)$. It is expedient to introduce the decomposition

$$T(m_z) = \tau_\varepsilon(m_z+1)\tau_\mu(m_z) \tag{36}$$

$$= \begin{pmatrix} 1 & 0 \\ \varepsilon(m_z+1) & 1 \end{pmatrix} \begin{pmatrix} 1 & \mu(m_z) \\ 0 & 1 \end{pmatrix}. \tag{37}$$

Further we can factorize the τ into a vacuum and a material contribution, $\tau_\varepsilon = \tau_{(\varepsilon-\varepsilon_{\text{vac}})}\tau_{\varepsilon_{\text{vac}}} = \tau_{\varepsilon_{\text{vac}}}\tau_{(\varepsilon-\varepsilon_{\text{vac}})}$ related to the polarization for the magnetic and analog for the electric field step. Note the renormalized vacuum permittivity $\varepsilon_{\text{vac}} = i\omega\varepsilon_0$ and permeability $\mu_{\text{vac}} = i\omega\mu_0$. As expected, $T(m_z)$ is unimodular. Now we can easily find the eigensystem; the eigensystem of the vacuum transfer matrix defines the plain wave basis on the lattice which we use to define the scattering formalism. Because of the unimodularity the two eigenvalues $\lambda = e^{\pm ik}$ are mutually reciprocal and for the propagating modes we are interested in on the unit circle, i.e., k is real. We get the characteristic polynomial $\lambda^2 - \lambda[2+\varepsilon_x(m_z+1)\mu_y(m_z)]+1$, hence $\cos k = 1+\varepsilon_x(m_z+1)\mu_y(m_z)/2$. The two signs of k correspond to the right- and left-moving waves. Note that ε and μ implicitly contain the ω dependence. To obtain the scattering matrix on the lattice we need the wave representation of the total transfer matrix of a unit cell. The right and left eigenvectors of $T(m_z)$ are distinct, $R_\lambda(m_z) = [1, (\lambda-1)/\mu_y(m_z)]^T$ and $L_\lambda(m_z) = [1, (\lambda-1)/\varepsilon_x(m_z+1)]^{*T}/(\lambda+1)^*$, and satisfy the orthogonality relation $L^+_{\lambda_i}(m_z)R_{\lambda_j}(m_z) = \delta_{ij}$. Note that we applied the common normalization to the left eigenvectors in order to normalize the electric field component of all right eigenvectors to 1. This is required for a clean definition of the scattering amplitudes analog to the continuum case. Further, the two right and the two left eigenvectors are linearly independent, respectively. Therefore we may group the two right and the two left eigenvectors of the vacuum transfer matrix into the matrices

$$\mathbf{L}_0^+ = \begin{pmatrix} \frac{1}{e^{ik}+1} & 0 \\ 0 & \frac{1}{e^{-ik}+1} \end{pmatrix} \begin{pmatrix} 1 & \frac{e^{ik}-1}{i\omega\varepsilon_0} \\ 1 & \frac{e^{-ik}-1}{i\omega\varepsilon_0} \end{pmatrix}, \tag{38}$$

$$\mathbf{R}_0 = \begin{pmatrix} 1 & 1 \\ \frac{e^{ik}-1}{i\omega\mu_0} & \frac{e^{-ik}-1}{i\omega\mu_0} \end{pmatrix}, \tag{39}$$

where the eigenvalues $\lambda = e^{\pm ik}$ satisfy the vacuum dispersion relation $2-2\cos k + \mu_{\text{vac}}\varepsilon_{\text{vac}} = 2-2\cos k - \omega^2\mu_0\varepsilon_0 = 0$ for the vacuum wave vector k, and use the projector $\mathbf{R}_0\mathbf{L}_0^+$ to obtain the wave representation of the total transfer matrix $\mathbf{T}_{\text{tot}}$ of the finite system as

$$\mathbf{T}_{\text{tot}}(k) = \mathbf{L}_0^+(k)\mathbf{T}_{\text{tot}}\mathbf{R}_0(k). \tag{40}$$

Then we get the usual definition of the scattering amplitudes from the correspondence between the scattering and the transfer matrix given by Eq. (5).

The homogeneous slab. Now we have to consider the total transfer matrix of our meta-materials. The most simple case is just a homogeneous slab of finite length. On the lattice, the composition of the total transfer matrix depends on the material discretization. We compute the total transfer matrix by starting from a right eigenvector of the vacuum base at the last vacuum site $m_z=0$ just before one side of the sample and apply successively the single-step transfer matrices $T(m_z)$ until we reach the first site $m_z=n+1$ right of the sample for which the $T(m_z)$ is a vacuum step again. We have n material layers inside the sample but $n+1$ transfer matrix step which depend on the material parameters μ_y, ε_x of the sample. Since we only have to consider a single polarization, we drop in the following the y,x indices in μ and ε in order to improve readability. Because in the discretized Maxwell equations the electric and magnetic fields live on mutual dual lattices, we distinguish three different single step $T(m_z)$ inside the sample instead of only one, as one would expect for a homogeneous slab. $T(m_z)$ depends on $\mu(m_z)$ and $\varepsilon(m_z+1)$. Therefore the first step $T(0)$ inside the sample sees only the electric response $\varepsilon(1)$ but no magnetic response of the material. The subsequent steps see both, ε and μ, and are constant across the bulk of the sample. The last step back into the vacuum behind the slab is special again. Both steps across the boundaries of the sample depend on the chosen material discretization. Here we adopt a symmetric material discretization[36] which respects the z isotropy such that the steps into and out of the sample become equal. Then we may calculate the wave representation as

$$\begin{aligned} T_{\text{tot}}(k) &= \mathbf{L}_0^+\tau_{\bar{\varepsilon}-\varepsilon}[\tau_\varepsilon\tau_\mu]^n\tau_{\bar{\varepsilon}-\varepsilon_{\text{vac}}}\tau_{\varepsilon_{\text{vac}}}\tau_{\mu_{\text{vac}}}\mathbf{R}_0 \\ &= \mathbf{L}_0^+\tau^{-1}_{\bar{\varepsilon}-\varepsilon_{\text{vac}}}\mathbf{R}[\mathbf{L}^+\tau_\varepsilon\tau_\mu\mathbf{R}]^n\mathbf{L}^+\tau_{\bar{\varepsilon}-\varepsilon_{\text{vac}}}T_{\text{vac}}\mathbf{R}_0 \\ &= [\mathbf{L}^+\tau_{\bar{\varepsilon}-\varepsilon_{\text{vac}}}\mathbf{R}_0]^{-1}[\mathbf{L}^+\tau_\varepsilon\tau_\mu\mathbf{R}]^n[\mathbf{L}^+\tau_{\bar{\varepsilon}-\varepsilon_{\text{vac}}}\mathbf{R}_0]T_{\text{vac}}(k), \end{aligned} \tag{41}$$

where $\{L_0^+, R_0\}$ is the eigenbase of the vacuum transfer matrix step T_{vacuum} with the eigenvalues $\lambda_0 = e^{\pm ik}$ as before, but $\{L^+, R\}$ now denotes the eigenbase of the transfer matrix step $\tau_\varepsilon\tau_\mu$ inside the homogeneous medium with the eigenvalues $\lambda = e^{\pm iq}$. We made use of the aforementioned identity $\tau_{\varepsilon_a}\tau_{\varepsilon_b} = \tau_{\varepsilon_a+\varepsilon_b}$. The symmetric material discretization introduces the averaged $\bar{\varepsilon} = (\varepsilon+\varepsilon_{\text{vac}})/2$ at the material's surface. As shown above, the wave vector in the vacuum k and inside the homogeneous slab q satisfy the dispersion relations $2-2\cos k + \mu_{\text{vac}}\varepsilon_{\text{vac}} = 0$ and $2-2\cos q + \mu\varepsilon = 0$. Since the matrix $\mathbf{L}^+\tau_\varepsilon\tau_\mu\mathbf{R}$ in Eq. (41) is diagonal, we basically have to calculate the matrix $\mathbf{L}^+\tau_{\bar{\varepsilon}-\varepsilon_{\text{vac}}}\mathbf{R}_0$. After some algebra we obtain for the homogeneous slab

$$T_{\mathrm{tot}}(k) = T_{\mathrm{core}}(k,n)T_{\mathrm{vacuum}}(k)$$

with the diagonal $T_{\mathrm{vacuum}}(k)$ and

$$T_{\mathrm{core}}(k,n) = \frac{1}{\zeta}\begin{pmatrix} \lambda^n G(\lambda) - \frac{1}{\lambda^n}G\left(\frac{1}{\lambda}\right) & \left(\lambda^n - \frac{1}{\lambda^n}\right)[2 - G(1)] \\ -\left(\lambda^n - \frac{1}{\lambda^n}\right)[2 - G(1)] & -\lambda^n G\left(\frac{1}{\lambda}\right) + \frac{1}{\lambda^n}G(\lambda) \end{pmatrix}, \tag{42}$$

where

$$G(\lambda) = \lambda\alpha(k) + \frac{\alpha(-k)}{\lambda} - \mu\varepsilon\alpha(k)\alpha(-k), \tag{43}$$

$$\alpha(k) = \frac{\varepsilon - \varepsilon_{\mathrm{vac}}}{2\varepsilon} + \frac{\lambda_0(k) - 1}{\varepsilon\mu_{\mathrm{vac}}}, \tag{44}$$

$$\zeta = \frac{(\lambda - \lambda^{-1})(\lambda_0 - \lambda_0^{-1})}{\varepsilon\mu_{\mathrm{vac}}}, \tag{45}$$

with $\alpha(k) + \alpha(-k) = 1$ and consequently $G(1) = 1 - \mu\varepsilon\alpha(k)\alpha(-k)$. Further we have $\alpha(k) - \alpha(-k) = \zeta/(\lambda - \lambda^{-1})$ and $G(\lambda) = G(\lambda^{-1}) + \zeta$. Note the antisymmetry of the off-diagonal elements. Using again the definition of the scattering matrix (5), we find the transmission and reflection amplitudes as

$$t_-(\omega,n) = \frac{\zeta\lambda_0}{\lambda^{-n}G(\lambda) - \lambda^n G(\lambda^{-1})},$$

$$r_+(\omega,n) = (\zeta\lambda_0)^{-1}(\lambda^n - \lambda^{-n})[2 - G(1)]t_-(\omega,n). \tag{46}$$

The nonvacuum factor of the lattice transfer matrix (42) appears to have the same symmetries as the transfer matrix of the homogeneous slab in the continuum: the off-diagonal terms are antisymmetric, the diagonal terms are mutual complex conjugates if $\varepsilon_{\mathrm{rel}}$ and μ_{rel} are real.

The periodic medium. Knowing the transfer matrix of the finite slab it is now easy to obtain the transfer matrix for a sample of multiple unit cells of the homogeneous as well as the periodic medium with the unit cell corresponding to Fig. 1(a). We can reduce the wave representation of the total transfer matrix to a product involving the wave representation of the homogeneous core we already know and some additional vacuum transfer matrix steps T_0 for the free space in the unit cell. We assume the measures a, b, and d in Fig. 1 to correspond to n_a, n_b, and n_d layers on the lattice. Then we get for the total transfer matrix of N unit cells of the periodic medium using $\tau_{\varepsilon_a+\varepsilon_b} = \tau_{\varepsilon_a}\tau_{\varepsilon_b}$ and, consequently, $\tau_{\bar{\varepsilon}-\varepsilon}\tau_{\bar{\varepsilon}-\varepsilon_{\mathrm{vac}}} = 1$

$$\begin{aligned} T_{\mathrm{pm},N}(k) &= \mathbf{L}_0^+[(\tau_{\varepsilon_{\mathrm{vac}}}\tau_{\mu_{\mathrm{vac}}})^{n_b}[\tau_{\bar{\varepsilon}}\tau_{\mu}(\tau_{\varepsilon}\tau_{\mu})^{n_d-1}\tau_{\bar{\varepsilon}}\tau_{\mu_{\mathrm{vac}}}] \\ &\quad\times(\tau_{\varepsilon_{\mathrm{vac}}}\tau_{\mu_{\mathrm{vac}}})^{n_a-1}]^N\tau_{\varepsilon_{\mathrm{vac}}}\tau_{\mu_{\mathrm{vac}}}\mathbf{R}_0 \\ &= [T_{\mathrm{vac}}{}^{n_b}(k)T_{\mathrm{core}}(k,n_d)T_{\mathrm{vac}}{}^{n_a}(k)]^N T_{\mathrm{vac}}(k) \end{aligned} \tag{47}$$

with the $T_{\mathrm{core}}(k,n_d)$ defined in Eq. (42). Since the phase factors $\lambda_0^{-(n_b-n_a)}$ and $\lambda_0^{n_b-n_a}$ introduced by the two vacuum slabs in the bracket on the last line of Eq. (47) do explicitly break the antisymmetry of the off-diagonal elements that is present for the single homogeneous slab in the continuum and, in the symmetric material discretization, also on the lattice, we can obtain a representation of the periodic medium by a homogeneous medium only for the case $n_b = n_a$. As already explained for the continuum case this is not a real restriction but instead just fixes the definition of the effective boundaries of the periodic medium. In the numeric simulation we have to explicitly compensate the corresponding vacuum phases in the scattering amplitudes. We can use the Chebyshev formula to explicitly calculate the Nth power such that we get the transmission and reflection amplitudes for the periodic medium after N unit cells in propagation direction as

$$t_-(\omega,N) = \lambda_0\left(\frac{\lambda^{-n_d}G(\lambda) - \lambda^{n_d}G(\lambda^{-1})}{\zeta\lambda_0^{n_b+n_a}}U_{N-1} - U_{N-2}\right)^{-1}, \tag{48}$$

$$r_+(\omega,N) = \frac{(\lambda^{n_d} - \lambda^{-n_d})[2 - G(1)]U_{N-1}t_-(\omega,N)}{\zeta\lambda_0^{n_a-n_b}\lambda_0}, \tag{49}$$

where the argument of the Chebyshev polynomials $U_N(p)$ is given by

$$p = \cos(qn_d)\cos[k(n_a + n_b)] - \frac{G(\lambda) + G(\lambda^{-1})}{\zeta}\sin(qn_d)\sin[k(n_a + n_b)]. \tag{50}$$

As for the continuum formulation, we actually get all the information about the metamaterial from the single unit cell. Comparing the scattering amplitudes (48) and (49) on the lattice with the normalized scattering amplitudes for homogeneous slab in the continuum tells us how to do the phase compensation for the lattice-TMM results $T = \lambda_0^{-1}t_-$ and $R = \lambda_0^{-(n_b-n_a)}r_+$. The condition for T arises from the additional vacuum step T_0 into the slab on the lattice, the compensation in R results from the symmetric definition of the boundary of the unit cell which is required to describe the periodic by a homogeneous medium as explained above.

Continuum HEM inversion. Again we ask whether the model periodic medium from Fig. 1 can be represented by an effective homogeneous medium. Here we have two choices: (i) we can compare the scattering amplitudes of the lattice periodic medium with the scattering formulas (21) and (22) derived for the homogeneous slab in the continuum or we can (ii) compare with the lattice scattering formulae for the homogeneous slab derived in this section. Moreover, we have to decide which material discretization to use. In this paper we will concentrate on comparing the lattice scattering results to the continuum scattering formulas for the homogeneous slab, as we previously did with the standard inversion procedure to obtain effective $\varepsilon_{\mathrm{eff}}(\omega)$ and $\mu_{\mathrm{eff}}(\omega)$ from the metamaterial simulations.

Analytically, the effective material parameters obtained from the HEM inversion for the lattice formulation of the model periodic media used in the last section to emulate the

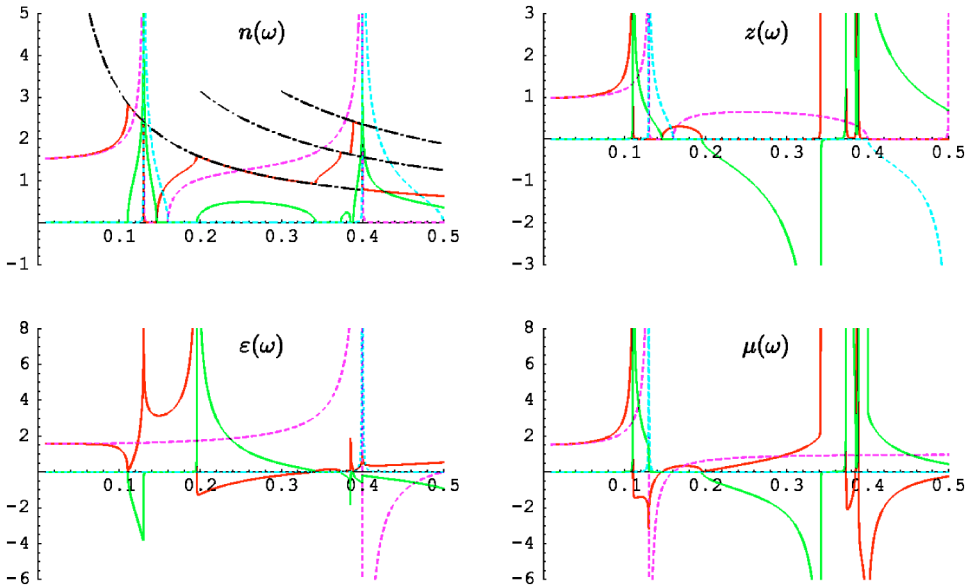

FIG. 3. (Color online.) The HEM inversion [Eqs. (10) and (11)] of the analytic lattice PEM scattering amplitudes [Eq. (46)] for model SRR-type material parameters $\omega_m=0.13$, $\omega_{mp}=0.16$ for the magnetic, and $\omega_e=0.4$, $\omega_{ep}=0.5$ for the electric response and $\gamma=10^{-4}$ [see Eqs. (29) and (30)]. The homogeneous core located in the middle of the unit cell was $d=L/10$ thick. The retrieved real (red, purple) and imaginary (green, turquoise) parts of effective parameters are shown as a function of frequency ω. Note the reduction of the multiple band gaps seen in Fig. 2 around the resonances to a single gap before each resonance. The dashed lines show the real (purple) and imaginary (turquoise) parts of the anticipated homogeneous parameters [Eqs. (29) and (30)] and corresponding index of refraction and impedance. The dash-dotted black lines in Re n_{eff} indicates the upper edge of the Brillouin zone $n_{\text{edge}}=k_{\text{edge}}/k=m\pi/(kL)$.

SRR and LHM metamaterials are shown in Figs. 3 and 4, respectively. As expected, the qualitative behavior is very similar to that found with the continuum formulation. All the problematic effects seen in the previously published simulations, such as resonance-antiresonance coupling, negative imaginary parts, deformed resonances, bad gaps, and so on, are present. The major difference to the continuum formulation becomes visible around the resonances. Where we previously found a series of tiny periodicity band gap around the resonances, in the lattice formulation we obtain a much

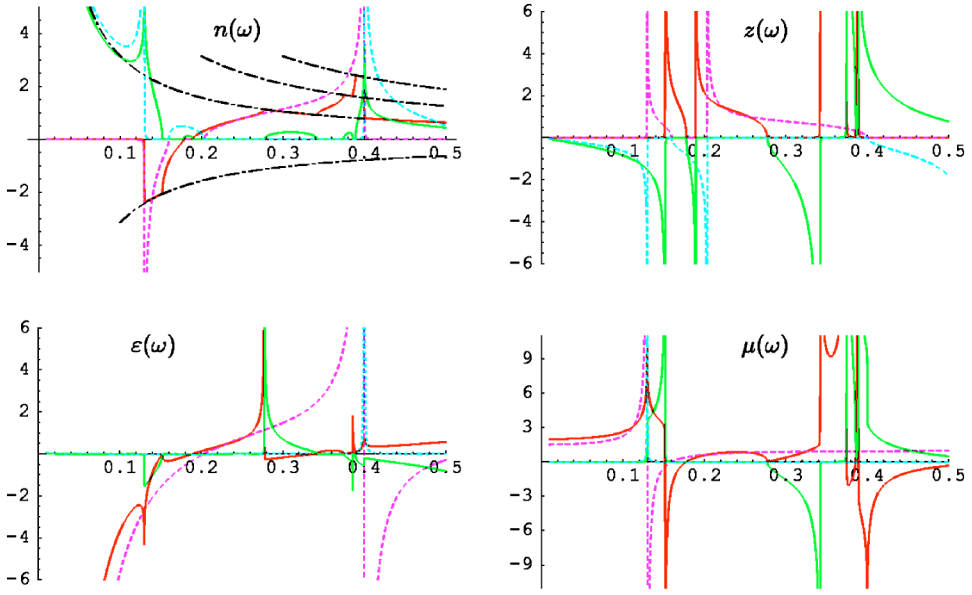

FIG. 4. (Color online.) The HEM inversion [Eqs. (10) and (11)] of the analytic lattice PEM scattering amplitudes [Eq. (46)] for model LHM-type material parameters $\omega_m=0.13$, $\omega_{mp}=0.16$ for the magnetic, and $\omega_e=0.4$, $\omega_{ep}=0.5$, $\omega_p=0.27$ for the electric response, and $\gamma=10^{-4}$ [see Eqs. (29) and (31)]. The homogeneous core located in the middle of the unit cell was $d=L/10$ thick. The retrieved real (red, purple) and imaginary (green, turquoise) parts of effective parameters are shown as a function of frequency ω. The dashed lines show the real (purple) and imaginary (turquoise) parts of the anticipated homogeneous parameters [Eqs. (29) and (31)] and corresponding index of refraction and impedance. The dash-dotted black lines in Re n_{eff} indicate the edges of the Brillouin zone, $n_{\text{edge}}=k_{\text{edge}}/k=m\pi/(kL)$.

TABLE I. Summary of the effective medium related acronyms.

HEM	Homogeneous effective medium, a homogeneous medium characterized by $\mu(\omega)$ and $\varepsilon(\omega)$ which, substituted for a finite metamaterial slab, length-independently reproduces (or approximates) the given scattering amplitudes.Here always used in continuum formulation. Finding a HEM for given *T*,*R*is called HEM inversion (if exact) or HEM approximation.
PEM	Periodic effective medium, a most simple periodic model-medium defined by $\mu_{\text{core}}(\omega)$,$\varepsilon_{\text{core}}(\omega)$ and a geometry shown in Fig. 1 which length-independently reproduces (or approximates) given scattering amplitudes. Also used a priori with given $\mu_{\text{core}}(\omega)$,$\varepsilon_{\text{core}}(\omega)$ to demonstrate effects of the periodicity. Here used in lattice formulation.
HEM(PEM)	The HEM which reproduces the scattering amplitudes calculated analytically from a given PEM.

simpler structure with basically one gap before each resonance. This is in excellent agreement with the numerical simulations, hence, expectedly, the lattice formulation compares much better to numerical simulations also obtained via discretization of the Maxwell equations than the continuum formulation. The discussion of further details we shall defer to a dedicated section below.

IV. SIMULATION RESULTS

In this section we now present actual TMM simulation results for real SRR and off-plane LHM metamaterials (see Table I). All numerical simulation are done using an implementation of the TMM method described by Markoš and Soukoulis.[12] The metamaterials are uniformly discretized on a cubic lattice using a symmetric material discretization. The dimensions of the unit cell are $6\times10\times10$ mesh steps, the single-ring SRR is a square ring of 7×7 mesh steps with a gap in the top side one mesh step wide. Propagation is for all cases along the SRR plane with the polarization of the incident plain wave such that the electric field is parallel to the two continuous sides of the SRR. Therefore we have only magnetic coupling to the magnetic resonance of the SRR.[5,35] Periodic boundary conditions apply to both directions perpendicular to the direction of propagation. For the off-plane LHM we add a one mesh-step thick continuous wire in front of the SRR such that the position of the wire is symmetric in the middle between two periodic repetitions of the SRR plane and centered with respect to the gap in the SRR. The direction of the wire is parallel to the continuous sides of the SRR, thus parallel to the incident electric field. All components of the metamaterials, the ring of the SRR and the continuous wire, are made from metal characterized by a constant relative permittivity of $\varepsilon_{\text{metal}}=(-3.0+5.88i)10^5$ and $\mu_{\text{metal}}=1$. Note that the results do not depend much on $\varepsilon_{\text{metal}}$ as long as it does not fall below a certain threshold.[12] The chosen value is reasonable to emulate metals such as Cu, Ag, Au in the range of GHz to a few THz. The rest of the unit cell is vacuum, there are no dielectric boards. The special geometry of the unit cell has been carefully chosen to preserve the inversion symmetry of the unit cell in the two directions perpendicular to the direction of propagation. This allows us to consider the scattering for only one polarization as it avoids complications by cross-polarization terms in the scattering amplitudes.[36] In this paper, we concentrate our consideration on the region around the magnetic resonance frequency ω_m, where we expect $\mu_{\text{eff}}(\omega)$ to become transitionally negative, for two reasons: first this is the region of interest for any left-handed application, and second, this is the frequency window for which simulation data is typically shown in the literature. A more detailed investigation of the higher frequency region, particularly the vicinity of the electric cut-wire response of the SRR and the intermediate periodicity band gaps will be published elsewhere.

In the following we show HEM inversion results for the scattering data numerically obtained for the metamaterial with the TMM. After the correct vacuum-phase compensation described above the inverted HEM scattering formulas (10) and (11) are applied to the simulated T and R for metamaterial slabs with a thickness of one, two, and three unit cell in propagation direction. We shall denote the results as $n_{\text{HEM}}(\omega)$ and $z_{\text{HEM}}(\omega)$ or $\mu_{\text{HEM}}=n_{\text{HEM}}z_{\text{HEM}}$ and $\varepsilon_{\text{HEM}}=n_{\text{HEM}}/z_{\text{HEM}}$, correspondingly. This approach is the same as chosen in the literature. Then we find the PEM approximation for the simulated metamaterial using the lattice formulation for the analytic scattering formula of a model periodic medium consisting of a homogeneous core which is a single discretization mesh-step thick and located the unit cell in the plain of the SRR gaps and the LHM continuous wire. This constitutes the lattice equivalent of a single scattering plain in the continuum. A model periodic medium, characterized by effective material constants $\mu(\omega)$ and $\varepsilon(\omega)$ of the homogeneous core, which reproduces the simulated T and R independent on the system length is called a periodic effective medium. The numeric inversion of the lattice scattering formulas (48) and (49) is applied to the simulated T and R for the first unit cell of each metamaterial, providing us with effective material constants $\mu_{\text{core}}(\omega)$ and $\varepsilon_{\text{core}}(\omega)$ for the homogeneous core of the PEM approximation. From the core parameters we can derive two further sets of effective parameters. First, we calculate the HEM inversion of the PEM scattering data obtained from the retrieved $\mu_{\text{core}}(\omega)$ and $\varepsilon_{\text{core}}(\omega)$ and compare the results with the HEM inversion of the direct simulation data to assess the quality of the PEM approximation. We denote this as HEM(PEM). Second, we introduce the material parameters $\mu_{\text{PEM}}(\omega)$ and $\varepsilon_{\text{PEM}}(\omega)$ of a homogeneous unit cell that would correspond to the PEM approximation in the effective medium limit, equating the total electric and magnetic polarizations of the respective unit cells

$$\mu_{\text{PEM}}(\omega) = 1 + \frac{n_d}{n_a + n_d + n_b}[\mu_{\text{core}}(\omega) - 1] \qquad (51)$$

and

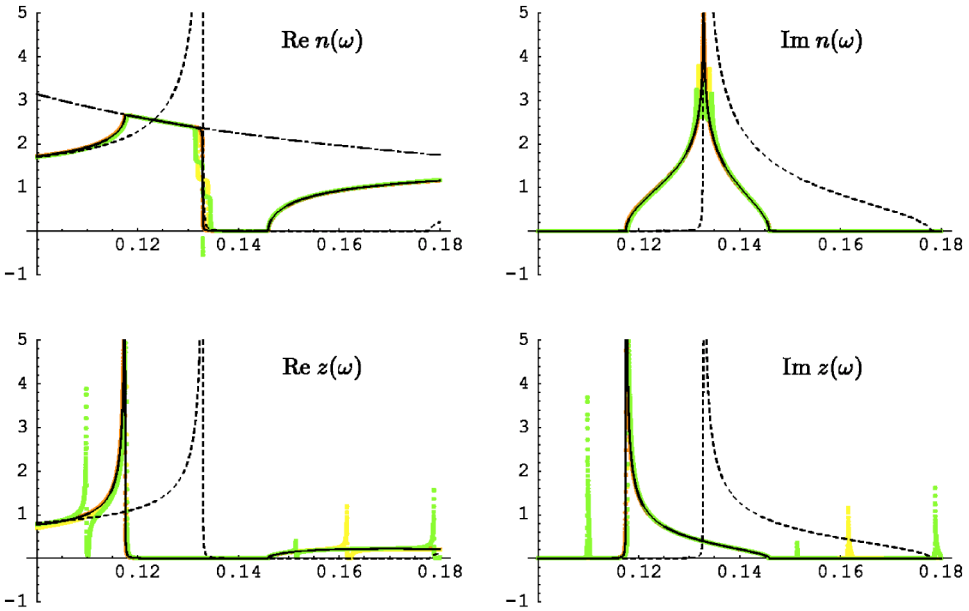

FIG. 5. (Color online.) For the simulated SRR metamaterial the effective index of refraction $n_{\mathrm{eff}}(\omega)$ and impedance $z_{\mathrm{eff}}(\omega)$ are shown. The colored curves represent the HEM approximation [Eqs. (10) and (11)] of the simulation data for the first three unit cells, the solid black line the HEM(PEM) approximation, and the dashed line the PEM approximation [see Eqs. (51) and (52)] obtained from the first unit cell data. Note the different positions of the resonance for $n_{\mathrm{eff}}(\omega)$ and $z_{\mathrm{eff}}(\omega)$.

$$\varepsilon_{\mathrm{PEM}}(\omega) = 1 + \frac{n_d}{n_a + n_d + n_b}[\varepsilon_{\mathrm{core}}(\omega) - 1]. \qquad (52)$$

The idea of this definition is to obtain parameters which we can compare with those of the HEM inversion, becoming equivalent with the latter if we can truly neglect the periodicity of the material. This allows us, to some degree, to consider the metamaterial's electromagnetic response as being composed of an actual contribution of the internal geometry of the metamaterials constituents and an explicit contribution of the periodic arrangement.

A. SRR

From the naive effective medium picture we expect the SRR to expose at the magnetic resonance brought about by the LC-oscillator-type response of the split ring to a perpendicular external magnetic field a Lorentz-type resonant form[4] in the permeability $\mu_{\mathrm{eff}}(\omega)$ but an unaffected, weakly frequency-dependent permittivity $\varepsilon_{\mathrm{eff}}(\omega)$. If the magnetic resonance is strong enough, i.e., the imaginary part in μ is small, we should find an isolated region where $\mathrm{Re}\,\mu_{\mathrm{eff}}(\omega) < 0$. The HEM approximation of the actual simulation data is shown as effective impedance $z_{\mathrm{HEM}}(\omega)$ and index of refraction $n_{\mathrm{HEM}}(\omega)$ in Fig. 5 as the colored points. The different colors (orange, yellow, green) correspond to different lengths of the metamaterial of one, two, and three unit cells in propagation direction. We see the typical behavior around ω_m we are already familiar with from previous work.[23] Instead of the expected form, we obtain a sharp cutoff in $\mathrm{Re}\,n_{\mathrm{HEM}}(\omega)$ on the low-frequency side, accompanied by a nonzero $\mathrm{Im}\,n_{\mathrm{HEM}}(\omega)$. The adjacent region with $\mathrm{Re}\,n_{\mathrm{HEM}} \approx 0$ and significant $\mathrm{Im}\,n_{\mathrm{HEM}} > 0$ should correspond to the negative μ produced by the magnetic resonance. Even more disturbing is the fact that the peaks in $z_{\mathrm{HEM}}(\omega)$ which should coincide with the peaks in $n_{\mathrm{HEM}}(\omega)$ directly at the resonance frequency ω_m do appear at substantially lower frequency. This behavior makes it hard to determine ω_m for the metamaterial since the retrieved $n_{\mathrm{HEM}}(\omega)$ and $z_{\mathrm{HEM}}(\omega)$ mutually disagree upon the value. We show that the HEM approximation of the metamaterial is, apart from some additional noise for longer systems, indeed length independent. Although we only show data for the first three unit cells we confirmed the length independence for all system lengths up to 11 unit cells. The dash-dotted line in Fig. 5(a) indicates the upper edge of the first Brillouin zone, $n_{\mathrm{edge}} = k_{\mathrm{edge}}/k = \pi/(kL)$, where L is the length of the unit cell in propagation direction. Clearly the cutoff of $\mathrm{Re}\,n_{\mathrm{HEM}}(\omega)$ coincides with this line. Note also that the peaks in $z_{\mathrm{HEM}}(\omega)$ appear exactly when $\mathrm{Re}\,n_{\mathrm{HEM}}(\omega)$ reaches $n_{\mathrm{edge}}(\omega)$. This behavior is generic, qualitatively the same is observed for different sizes of the unit cell and different geometries of the SRR, including single-ring and double-ring SRRs as well as more symmetric multigap SRRs.[22] The corresponding effective permittivity and permeability of the HEM approximation are shown in Fig. 6. Again, the colored points represent the simulation data for one to three unit cells. The most striking deviation from the expected effective medium behavior is the resonance-antiresonance coupling between $\mathrm{Re}\,\mu_{\mathrm{HEM}}(\omega)$ and $\mathrm{Re}\,\varepsilon_{\mathrm{HEM}}(\omega)$, accompanied by a significant negative imaginary part of the permittivity, $\mathrm{Im}\,\varepsilon_{\mathrm{HEM}}(\omega) < 0$. Moreover, the negative region of the μ resonance is strongly but characteristically deformed and not ascending monotonically from a negative divergency. Of course, the divergencies of the effective parameters would be blurred in the presence of large imaginary parts in μ or ε, but at least for our simulations using almost perfect metals in vacuum we would expect reasonably sharp divergencies. As a consequence of the length independence of n_{HEM} and z_{HEM} also the retrieved $\mathrm{Re}\,\mu_{\mathrm{HEM}}(\omega)$ and $\mathrm{Re}\,\varepsilon_{\mathrm{HEM}}(\omega)$ are basically length independent.

In the analytic sections above we demonstrated that the periodicity can produce all that kind of effects violating the effective medium picture in our simulations. Now we show that the PEM approximation of the simulation data yields reasonable effective parameters free of the above artifacts.

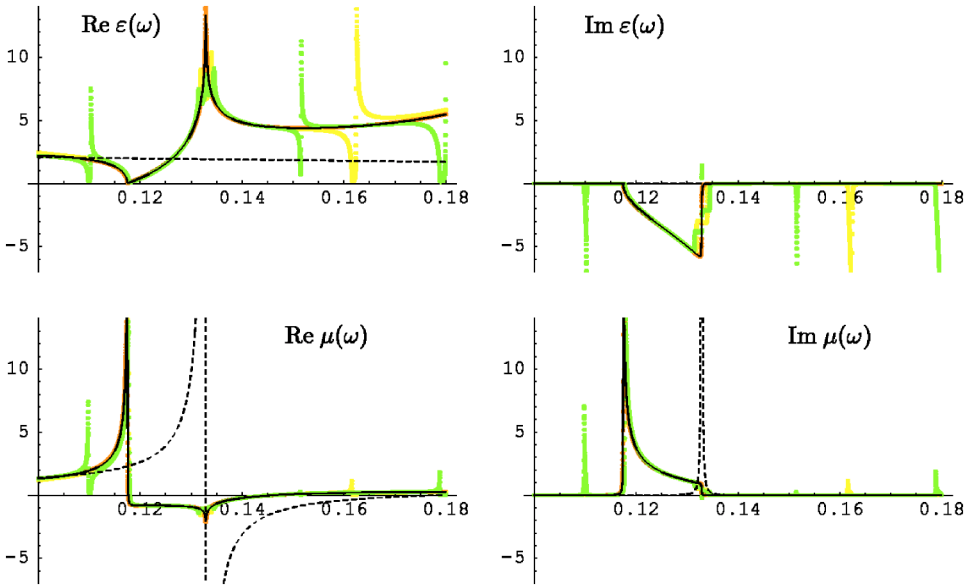

FIG. 6. (Color online.) For the simulated SRR metamaterial the effective permittivity $\varepsilon_{\text{eff}}(\omega)$ and permeability $\mu_{\text{eff}}(\omega)$ are shown. The colored curves represent the HEM approximation [see Eqs. (10) and (11)] of the simulation data for the first three unit cells, the solid black line the HEM(PEM) approximation, and the dashed line the PEM approximation [Eqs. (51) and (52)] obtained from the first unit cell data. Note the antiresonant behavior of the permittivity and the misshapen magnetic resonance in the frequency interval where $n_{\text{eff}}(\omega)$ reaches the edge of the Brillouin zone.

The dashed curves in Figs. 5 and 6 represent the effective parameters $\mu_{\text{PEM}}(\omega)$ and $\varepsilon_{\text{PEM}}(\omega)$, with the corresponding $n_{\text{PEM}}(\omega)$ and $z_{\text{PEM}}(\omega)$, extracted from the PEM approximation of the simulation data as described above. For the PEM unit cell we chose $n_a=5$, $n_d=1$, and $n_b=4$ to fit the symmetry of the metamaterials unit cell that embeds the $1\times7\times7$ SRR into a $6\times10\times10$ unit cell. From the corresponding $\mu_{\text{core}}(\omega)$ and $\varepsilon_{\text{core}}(\omega)$ we can in turn calculate the scattering amplitudes of the PEM and subject those to the HEM inversion. The resulting HEM(PEM) parameters are shown as the solid black lines which virtually coincide with the first unit cells simulated HEM parameters, hence basically also with those of the longer systems, proving that the PEM approximation is reliable. Obviously the PEM parameters behave exactly as we expected from the effective medium picture in the first place. There is a clean resonance in $n_{\text{PEM}}(\omega)$ and the peaks of $n_{\text{PEM}}(\omega)$ and $z_{\text{PEM}}(\omega)$ now appear at the same frequency, rendering ω_m well defined. There is no resonance-antiresonance coupling between $\mu_{\text{PEM}}(\omega)$ and $\varepsilon_{\text{PEM}}(\omega)$ anymore. The permittivity is roughly constant across ω_m and does not show any negative imaginary part. The permeability $\mu_{\text{PEM}}(\omega)$ exposes a clear, antisymmetric resonance at ω_m in its real part in conjunction with a symmetric absorption peak in the imaginary part at the same frequency. Note further that the frequency ω_{mp} where Re $\mu_{\text{HEM}}(\omega)$ get back to positive values after the magnetic resonance is substantially smaller than the corresponding frequency for Re $\mu_{\text{PEM}}(\omega)$. The procedure yields analogue results for different SRR geometries and different size of the unit cell (not shown).

Effective medium behavior was expected in the first place because the vacuum wavelength of the incident radiation at the magnetic resonance frequency ω_m is large compared to the size of the unit cell for the customary LH and related metamaterials. In most experiments and simulations this ratio is in the range of ten to five.[5–7,10,13,22,23,28,37–39] In the SRR metamaterial presented above we went intensionally to the lower extreme to make the effects of the periodicity more pronounced and more easy to identify. In Figs. 7 and 8 we present the analog HEM and PEM approximation results for a SRR with five times lower ω_m. The size of the SRR and the unit cell are kept constant. To lower the resonance frequency of a SRR without changing the size one would usually decrease the width of the gap in the SRR increasing its capacitance. Due to the limitations of the used TMM implementation (uniform discretization) this was not feasible. Therefore we adopted the alternative possibility to place some high dielectric constant material inside the SRR gap, which serves the same purpose and can be used to emulate a narrower gap. For this low-frequency SRR the wavelength to unit cell size ratio around ω_m is roughly 25, higher than in any published LHM. The behavior of the retrieved effective $n_{\text{HEM}}(\omega)$ and $z_{\text{HEM}}(\omega)$ in Fig. 7 is now qualitatively as expected from the effective medium picture, the refractive index and impedance of the HEM approximation virtually coincide with the PEM parameters $n_{\text{PEM}}(\omega)$ and $z_{\text{PEM}}(\omega)$. As the magnetic resonance is now shifted far below the edge of the Brillouin zone there is no visible cutoff in Re $n_{\text{HEM}}(\omega)$ and the resonance peaks in n and z appear at the same frequency ω_m. Note that $\mu_{\text{HEM}}(\omega)$ reaches unity away from ω_m to either side. Also the effective permeabilities of HEM and PEM in Fig. 8 do coincide, exposing a clean antisymmetric resonance in Re μ and a symmetric positive absorption peak in Im μ. Surprisingly, though weak there is still a noticeable residue of the resonance-antiresonance coupling left in Re $\varepsilon_{\text{HEM}}(\omega)$ together with the corresponding negative imaginary part. Only here the HEM approximation deviates from the PEM approximation which expectedly does not show these effects. All effective parameters are almost perfectly length independent. This has been verified for up to 10 unit cells in propagation direction (not shown). Note also the absence of the additional noise observed in the effective parameters for longer systems. These results show that the artifacts in the HEM approximation which we identified as effects of the metamaterial's periodicity vanish if we approach the effective medium limit. At low frequencies HEM and PEM approximation converge, however, even in this extreme low-frequency limit remains of the periodicity artifacts are still visible. Since for virtually all the metamaterials measured or simulated that have been

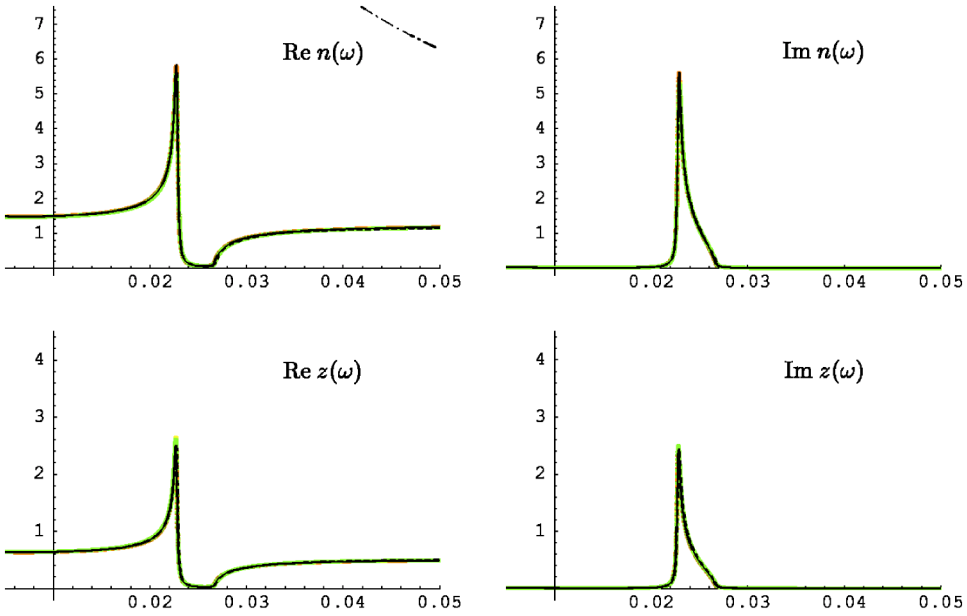

FIG. 7. (Color online.) For the simulated low-frequency SRR metamaterial the effective index of refraction $n_{\text{eff}}(\omega)$ and impedance $z_{\text{eff}}(\omega)$ are shown. The colored curves represent the HEM approximation [Eqs. (10) and (11)] of the simulation data for the first three unit cells, the solid black line the HEM(PEM) approximation, and the dashed line the PEM approximation [see. Eqs. (51) and (52)] obtained from the first unit cell data. Note that far away from the edge of the Brillouin zone HEM and PEM approximation, and the expected homogeneous medium behavior coincide.

published the wavelength to unit cell size ratio is worse than 25, we expect the metamaterial's periodicity required to be taken into account.

B. LHM

The most simple way to obtain a left-handed material is to add an appropriately dimensioned[29,40] continuous wire to the SRR considered above. From the naive effective medium picture we expect for the LHM a Lorentz-type resonance in μ in combination with a plasmonic form, modified by the electric cut-wire response of the SRR where necessary,[29] which is essentially negative around the magnetic resonance frequency ω_m. The effective impedance and index of refraction of the HEM approximation for the first three unit cells of the LHM in propagation direction is shown in Fig. 9 as the colored points. In violation of the assumed effective medium picture we find again a cutoff of the negative resonant $\text{Re}\, n_{\text{HEM}}(\omega)$ this time at the lower edge of the first Brillouin zone $n_{\text{edge}}=-k_{\text{edge}}/k=-\pi/(kL)$, where L is the length of the unit cell in propagation direction. The imaginary part of n does not have the expected form either. In $z_{\text{HEM}}(\omega)$ we expect two peaks for the LHM, one at ω_m and another one at the electric (effective) plasma frequency ω_p' which is the lowest frequency where $\varepsilon(\omega)$ becomes positive. Though the retrieved $z_{\text{HEM}}(\omega)$ does show two such peaks, the position of the first one associated with ω_m does not agree with the ω_m derived from $n_{\text{HEM}}(\omega)$. This is the same issue as found for the SRR above. The corresponding effective permeability $\mu_{\text{HEM}}(\omega)$ and permittivity $\varepsilon_{\text{HEM}}(\omega)$ are shown in Fig. 10. The

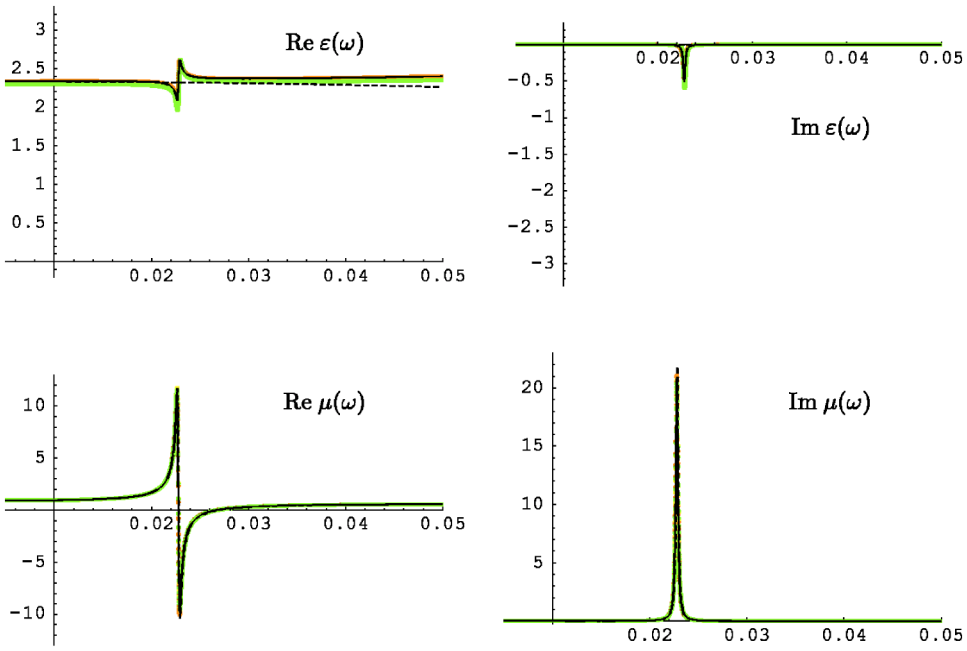

FIG. 8. (Color online.) For the simulated low-frequency SRR metamaterial the effective permittivity $\varepsilon_{\text{eff}}(\omega)$ and permeability $\mu_{\text{eff}}(\omega)$ are shown. The colored curves represent the HEM approximation [see. Eqs. (10) and (11)] of the simulation data for the first three unit cells, the solid black line the HEM(PEM) approximation, and the dashed line the PEM approximation [Eqs. (51) and (52)] obtained from the first unit cell data. In the low-frequency limit the resonance/antiresonance coupling as well as the negative imaginary parts disappear.

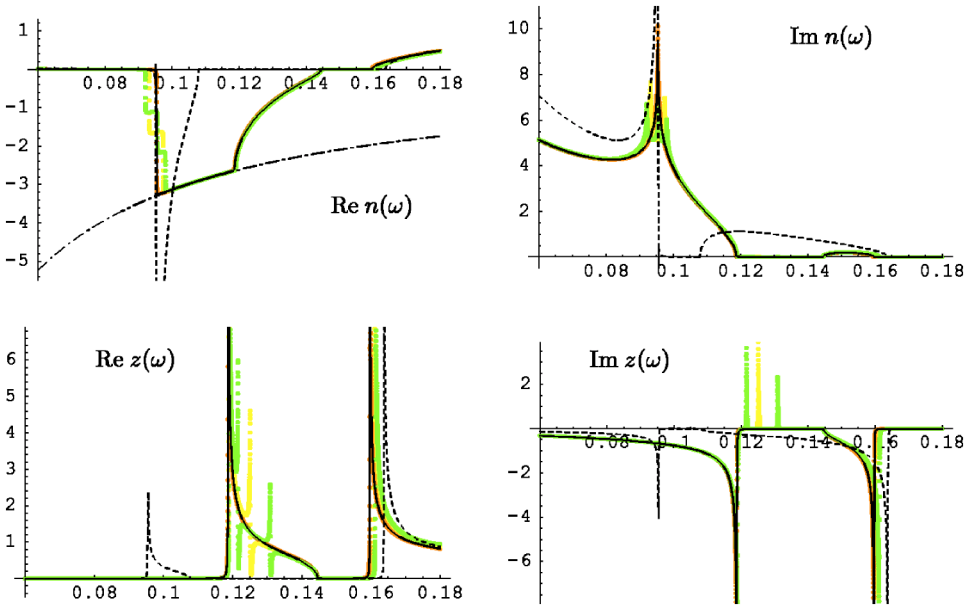

FIG. 9. (Color online.) For the simulated off-plane LHM metamaterial the effective index of refraction $n_{\text{eff}}(\omega)$ and impedance $z_{\text{eff}}(\omega)$ are shown. The colored curves represent the HEM approximation [Eqs. (10) and (11)] of the simulation data for the first three unit cells, the solid black line the HEM(PEM) approximation, and the dashed line the PEM approximation [see. Eqs. (51) and (52)] obtained from the first unit cell data.

previously published resonance-antiresonance coupling in the real parts around ω_m is clearly visible, together with the appearance of the negative imaginary part in the permittivity and the misshapen absorption peak in the permeability. Also for the LHM we can now confirm the length independence of the HEM approximation, apart from some additional noise, up to 10 unit cells in propagation direction. As for the SRR the PEM approximation of the LHM yields effective parameters free of all the artifacts seen in the HEM parameter which demonstrates again their origin in the periodic structure of the metamaterial. In $n_{\text{PEM}}(\omega)$ and $z_{\text{PEM}}(\omega)$ we obtain an untruncated magnetic resonance and agreement of n and z upon the position of ω_m. The permittivity $\varepsilon_{\text{PEM}}(\omega)$ and permeability $\mu_{\text{PEM}}(\omega)$ show a clean magnetic resonance with a symmetric absorption peak and the anticipated electric plasmonic behavior without any negative imaginary parts. In $\varepsilon_{\text{PEM}}(\omega)$ we can even recognize the beginning ascent of the imaginary part to the absorption peak at $\omega=0$ contributed by the plasma resonance of the continuous wire. Note again the shift in ω_{mp} while the electric plasma frequency ω_p' is essentially the same for HEM and PEM approximation, although the descent to negative values for decreasing frequency is more rapid for $\varepsilon_{\text{PEM}}(\omega)$. Also for the LHM these results are generic, i.e., have been qualitatively reproduced for different sizes of the SRR and continuous wire components of the LHM and the unit cell.

C. Continuous wire and cut wire

Not only the behavior of the SRR based metamaterials around the magnetic resonance but also that of the periodic arrangement of continuous wires or cutwires are strongly affected by the periodicity. In the effective medium picture, the continuous wire is expected to expose a simple plasmonic permittivity going monotonously from negative to positive real part and crossing zero at a single plasma frequency ω_p.

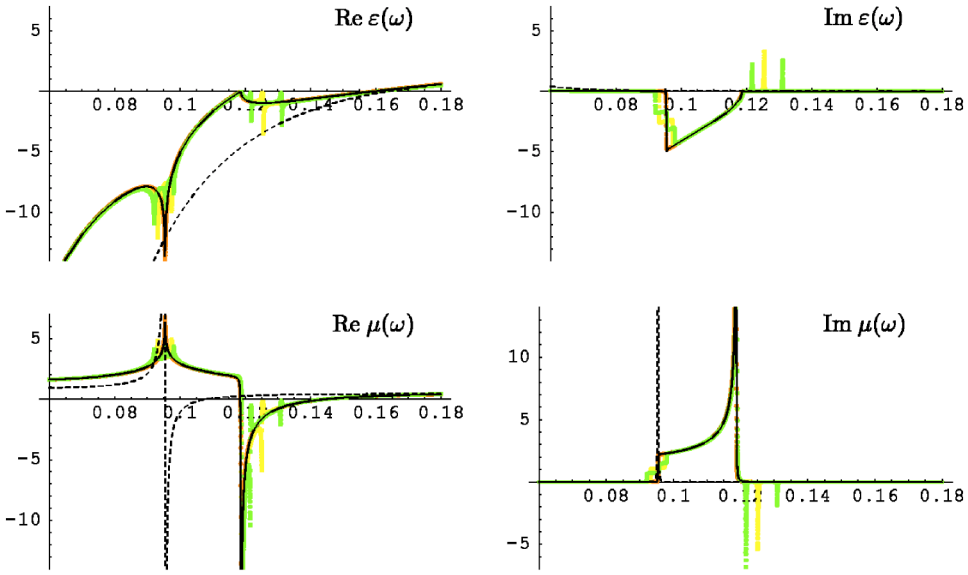

FIG. 10. (Color online.) For the simulated off-plane LHM metamaterial the effective permittivity $\varepsilon_{\text{eff}}(\omega)$ and permeability $\mu_{\text{eff}}(\omega)$ are shown. The colored curves represent the HEM approximation [see. Eqs. (10) and (11)] of the simulation data for the first three unit cells, the solid black line the HEM(PEM) approximation, and the dashed line the PEM approximation [Eqs. (51) and (52)] obtained from the first unit cell data.

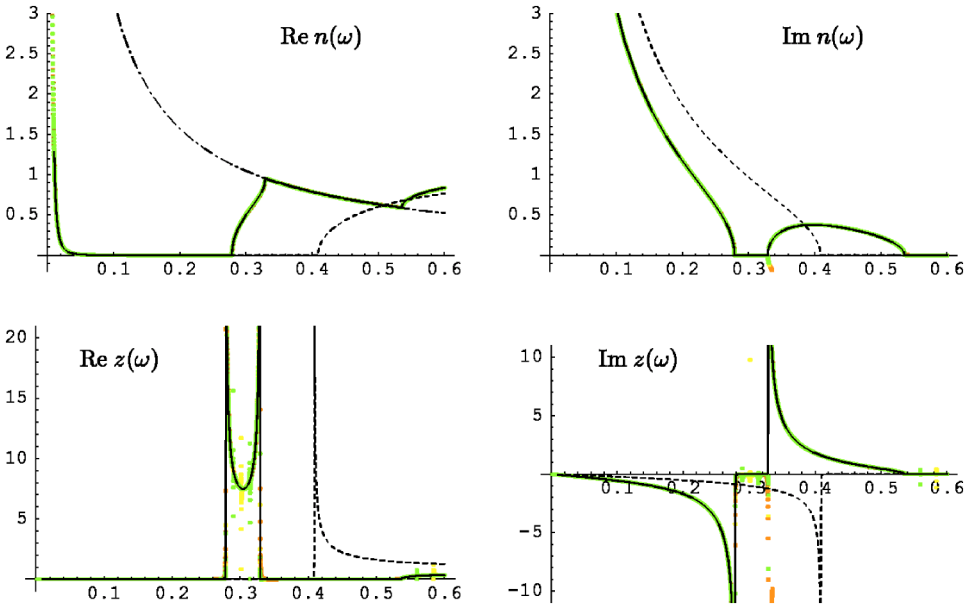

FIG. 11. (Color online.) For the simulated continuous wire metamaterial the effective index of refraction $n_{\mathrm{eff}}(\omega)$ and impedance $z_{\mathrm{eff}}(\omega)$ are shown. The colored curves represent the HEM approximation [Eqs. (10) and (11)] of the simulation data for the first three unit cells, the solid black line the HEM(PEM) approximation, and the dashed line the PEM approximation [see Eqs. (51) and (52)] obtained from the first unit cell data.

In the HEM approximation of simulated continuous wire metamaterials,[2] e.g., the isolated continuous wire array from the LHM discussed above, we observe the anticipated plasmonic behavior only at low frequencies up to the order of the plasma frequency ω_p of the wire. At higher frequency we find a sequence of additional stop bands which can be explained as periodicity band gaps in the framework of the PEM model: whenever the residue class $\mathrm{Re}\, n(\omega) \mathrm{mod}\, 2\pi/k$ comes close to the edge of the first Brillouin zone a periodicity band gap is opened where a representative of $\mathrm{Re}\, n_{\mathrm{HEM}}(\omega)$ follows the line $n_{\mathrm{edge}}(\omega)$ and $\mathrm{Im}\, n_{\mathrm{HEM}}(\omega)$ is significantly nonzero. At the boundaries of each of these band gaps the real and the imaginary part of the effective impedance $z_{\mathrm{HEM}}(\omega)$ have either a zero or a pole which leads to the appearance of an alternating sequence of phony resonance-like structures in $\mu_{\mathrm{HEM}}(\omega)$ and $\varepsilon_{\mathrm{HEM}}(\omega)$. The corresponding series of transmission above the "first" ω_p have also been confirmed in experiments[41] with thin metallic wires on PCB boards. Using the PEM approximation of the simulation data we can describe the scattering amplitudes in terms of a $\varepsilon_{\mathrm{PEM}}(\omega)$ which does possess just the expected plasmonic form in conjunction with an almost exactly $\mu_{\mathrm{PEM}}(\omega)=1$. The plasma frequency in $\varepsilon_{\mathrm{HEM}}(\omega)$, however, does not coincide with the "lowest" ω_p of the HEM approximation but appears moderately shifted to higher frequency. The HEM and PEM approximation for a metamaterial comprising a periodic array of continuous thin wires parallel to the electric field of the incident electromagnetic wave is shown in Figs. 11 and 12. Both effective material approximations are virtually independent on the system length.

The periodic array of cut wires is of interest for two reasons: first, it can be used as a model of the electric response of the SRR and second, we could substitute the continuous wire in the LHM to tailor the collective $\varepsilon_{\mathrm{eff}}(\omega)$ or to simplify its mechanical construction. For a sufficiently low resonance frequency ω_e the cut wire shows a behavior analogous to the

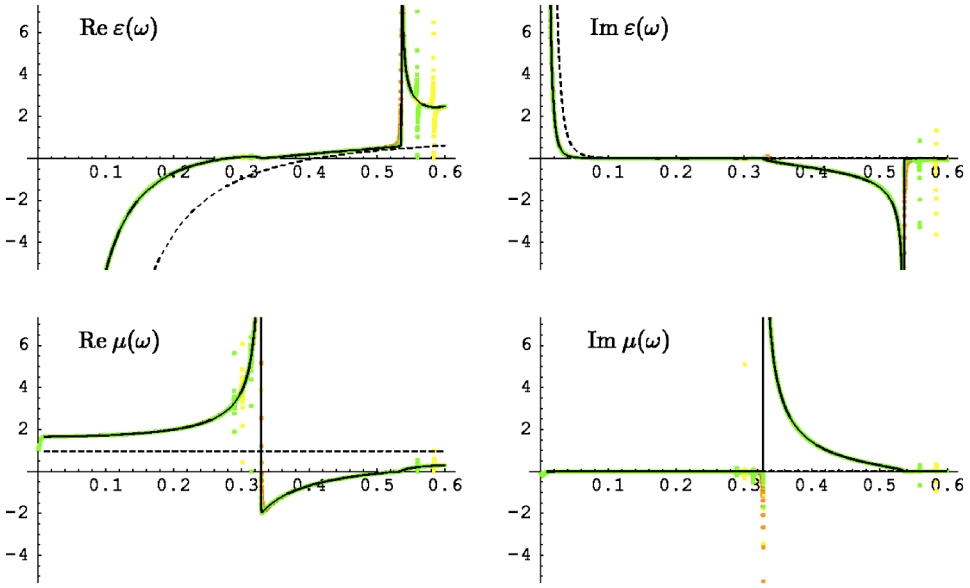

FIG. 12. (Color online.) For the simulated continuous wire metamaterial the effective permittivity $\varepsilon_{\mathrm{eff}}(\omega)$ and permeability $\mu_{\mathrm{eff}}(\omega)$ are shown. The colored curves represent the HEM approximation [see Eqs. (10) and (11)] of the simulation data for the first three unit cells, the solid black line the HEM(PEM) approximation, and the dashed line the PEM approximation [Eqs. (51) and (52)] obtained from the first unit cell data.

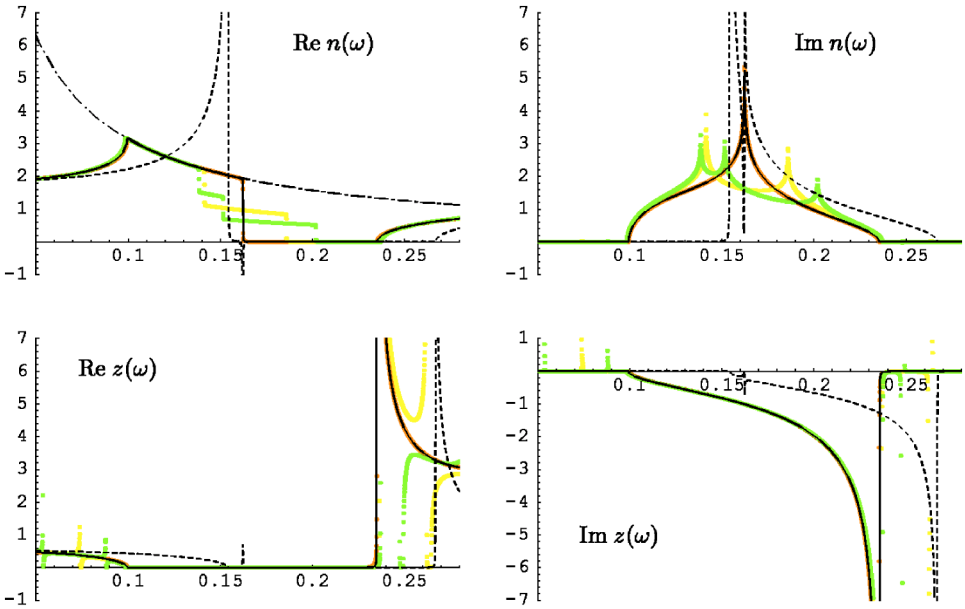

FIG. 13. (Color online.) For the simulated cut-wire metamaterial the effective index of refraction $n_{\mathrm{eff}}(\omega)$ and impedance $z_{\mathrm{eff}}(\omega)$ are shown. The colored curves represent the HEM approximation [Eqs. (10) and (11)] of the simulation data for the first three unit cells, the solid black line the HEM(PEM) approximation, and the dashed line the PEM approximation [see Eqs. (51) and (52)] obtained from the first unit cell data. The weak additional structure in the PEM approximation close to the resonance is indicating the beginning breakdown of the approximation of the metamaterial within our most simple periodic medium model.

SRR but with the electric and magnetic parameters exchanged. We observe[23] all the previously described artifacts in the HEM approximation: the resonance-antiresonance coupling, where the (electric) resonance appears this time in $\varepsilon_{\mathrm{HEM}}(\omega)$, accompanied by a negative imaginary part in $\mu_{\mathrm{HEM}}(\omega)$, the cutoff of $n_{\mathrm{HEM}}(\omega)$ at the Brillouin zone edge, and so on. However, since in real metamaterials the cut-wire resonance usually appears at much higher frequency, we observe an additional periodicity band gap at lower frequency, well separated from the cut-wire response, qualitatively as shown in Fig. 3. The effective parameters $\mu_{\mathrm{HEM}}(\omega)$ and $\varepsilon_{\mathrm{HEM}}(\omega)$ at the lower boundary of this additional band gap will appear very similar to those of a cut-wire resonance at low frequency ω_e. Note that we can shift the cut-wire resonance to arbitrarily low frequency by reducing the gap in the longitudinal direction of the cut-wires, i.e., making the finite wires almost as long as the width of the unit cell. The HEM and PEM approximation for such a metamaterial of cut wires parallel to the electric field of the incident electromagnetic wave is shown in Figs. 13 and 14. In either case, the effective parameters obtained from the PEM approximation basically do not show any artifacts around the cut-wire resonance nor the periodicity band gaps and behave very much as expected from the naive effective medium picture. This gives us a criterion to distinguish the real cut-wire resonance in a metamaterial from the possible phony one brought about by the periodicity.

V. DISCUSSION

When Veselago conceived the idea of heft-handed electromagnetic material he essentially considered theoretical homogeneous media for which there are no correspondents in nature. Though there are materials exposing a negative magnetic response and other materials with a negative electric response, the challenge is to obtain both simultaneously in a

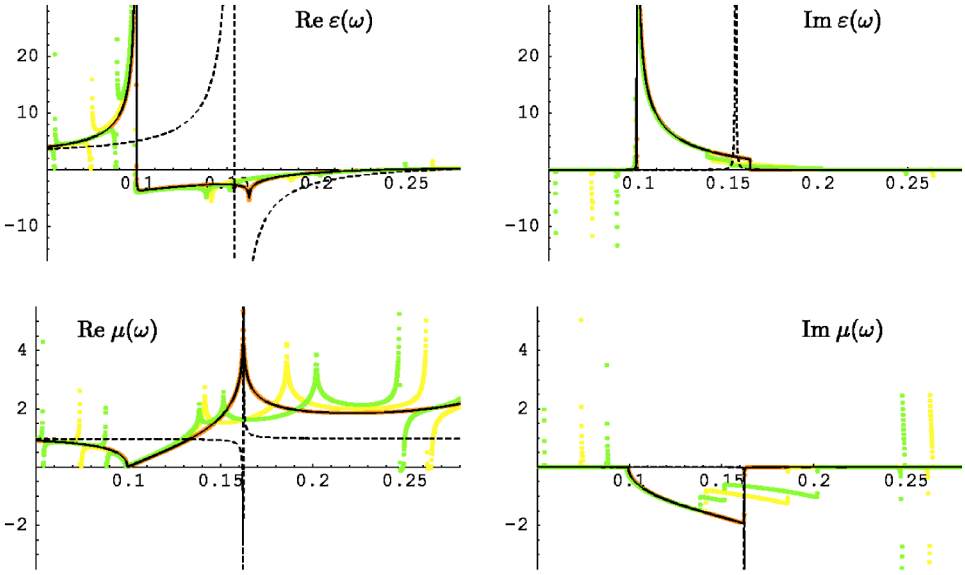

FIG. 14. (Color online.) For the simulated cut-wire metamaterial the effective permittivity $\varepsilon_{\mathrm{eff}}(\omega)$ and permeability $\mu_{\mathrm{eff}}(\omega)$ are shown. The colored curves represent the HEM approximation [see Eqs. (10) and (11)] of the simulation data for the first three unit cells, the solid black line the HEM(PEM) approximation, and the dashed line the PEM approximation [Eqs. (51) and (52)] obtained from the first unit cell data.

material and, moreover, at an experimentally useful frequency in or above the microwave range. After Pendry proposed the first practical possibility to obtain controllable resonant magnetic and plasmonic negative electric response by the means of the geometric shape of electric conductors (SRR and continuous wire) in a periodic arrangement, numerical simulations have been conducted, attempting to verify the simultaneous negative magnetic and electric response. Note that because of the technical difficulty to obtain reliable complex reflection amplitudes from experimental measurements numerical simulations are here the most important tool to address the question of negative electromagnetic response. The existence of negative refraction, which is merely a consequence of an antiparallel phase and group velocity, has been demonstrated experimentally but provides no proof for the actual Veselago picture of simultaneously negative μ and ε. For this purpose, at typical vacuum wavelengths of around ten times the size of the unit cell effective medium behavior of the metamaterials has been assumed throughout the literature such that an effective permeability and permittivity could be obtained in a HEM approximation. Although the working frequency of a SRR-based LHM is theoretically arbitrary, the fabrication technique in experiments and the limited computer power in numerical simulations impose certain constraints on the size of the smallest structures (particularly the width of the gap in the SRR) in comparison to the size of the unit cell. As a consequence the ratio of the vacuum wavelength around the magnetic resonance to the size of the unit cell is confined as well.

Continuum HEM approximation. The effective refractive index $n_{\mathrm{HEM}}(\omega)$, impedance $z_{\mathrm{HEM}}(\omega)$ and, derived from those, permeability $\mu_{\mathrm{HEM}}(\omega)$ and permittivity $\varepsilon_{\mathrm{HEM}}(\omega)$ published by us[13,14,20,23] and others[9,19,21,22] for the LHM, SRR, and cut-wire metamaterials do only in first approximation meet the anticipated effective response of the material. For the considered polarization (electric field parallel to the continuous wire and perpendicular to the gap bearing side of the SRR) and direction of propagation in the SRR plane the resonant circulating currents inside the SRR ring should couple and respond only to the magnetic field, affecting the behavior of the effective $\mu(\omega)$. The electric field couples to the continuous wire or cut wire. However, it also couples to a separate electric resonance of the SRR caused by induced polarization currents oscillating linearly in the gapless sides of the SRR which are parallel to the electric field. For other orientations, due to the anisotropy arising from the gap in the SRR ring, the electric field may also couple to the resonance of the circulating currents making the total effective behavior a lot more complicated. In some cases violating the inversion symmetry of the unit cell also a magnetic coupling to the electric cut-wire response is possible. Though we obtain from the simulations a resonant magnetic (magnetic resonance frequency ω_m for SRR, LHM) and electric (cut-wire resonance frequency ω_e for SRR, cut wire) response as well as basically the plasmonic response of the continuous wire and its corresponding contribution in the LHM, the correspondence to the effective medium picture is spoiled by partially very significant anomalies. (i) Resonance-antiresonance coupling. We expect the electric and magnetic response of the discussed metamaterials to be independent. However, whenever there is a resonance in $\mathrm{Re}\,\mu$ we simultaneously observe an antiresonant behavior in $\mathrm{Re}\,\varepsilon$, and vice versa. The antiresonant structures in the real part are accompanied by a negative imaginary part. (ii) Misshapen, truncated resonances. The divergence in $\mathrm{Re}\,n$ appears to be cut off at the edges of the first Brillouin zone and, in particular, the negative regions of the magnetic resonance in μ and cut-wire resonance in ε do not return from large negative real part but seem to saturate in a rather shallow behavior. The corresponding absorption peak in the imaginary parts as misshapen and highly asymmetric too. (iii) Discrepancy between n and z about the positions of the resonances. We expect the peaks (or zeros) in the index of refraction and the impedance to appear exactly at the resonance frequencies ω_m and ω_e, or the effective plasma frequency ω_p'. From the simulations, however, we find different frequencies from n and z, respectively. This led for instance to an "internal structure" of the magnetic resonance as shown in Fig. 5, which can not easily be explained within the assumed effective medium picture. (iv) Additional spectral structures. Apart from structures around the anticipated contributions of the metamaterial's constituents ω_m, ω_e, and ω_p' we observe a lot of additional structure, especially at higher frequency, which can not be accounted for. The observed artifacts in the HEM approximations are quite generic and have meanwhile been reported by different groups. An explanation for all these effects is given by the periodicity, see below.

The occurrence of negative imaginary parts the permittivity or permeability has been criticized by several authors.[24–26] Indeed, a physical, passive homogeneous material may not possess any negative imaginary in μ and ε. As long as the material is passive, it can only absorb energy from the electromagnetic field. If there was any negative imaginary part in μ or ε one could devise a geometry of this material which would violate the passivity. This requirement does not apply to the HEM approximation. The *effective* material is defined as the homogeneous material which reproduces the scattering amplitudes of the metamaterial within the given geometry, i.e., normal incidence to a homogeneous slab of finite length in propagation direction, if a length independent solution does exist. Our retrieved HEM parameters provide such a length independent description of the actual scattering amplitudes of the metamaterial. For the (stationary) scattering of plain waves at a finite homogeneous slab in the continuum there are μ and ε with negative imaginary parts which do not violate the passivity of the material, as long as much weaker conditions $\mathrm{Im}\,\mu+\mathrm{Im}\,\varepsilon \geqslant 0 \wedge \mathrm{Im}\,\mu/|\mu|+\mathrm{Im}\,\varepsilon/|\varepsilon| \geqslant 0$ are satisfied. If we further restrict the scattering setup requiring the thickness of slab to be an integral multiple of the unit cell, which is reasonable for this type of metamaterial, we have even more freedom in μ and ε. The HEM approximation is only valid for a given geometry, there is not necessarily a physical material exposing the same material parameters in an arbitrary setup.

Some authors[42] have suggested a more general effective description[43] of the metamaterials which employ tensorial μ and ε to take the coupling of the electric field to, and the anisotropy of the SRR into account. Though this is certainly an issue for arbitrary orientation of the SRR and will gain importance in more-dimensional materials, it is not directly

related to the deviations from the effective medium behavior discussed above.

Apart from some additional "noise," we could confirm the length independence of the HEM approximation for all considered metamaterials up to 11 unit cells in propagation direction. In contrast to previous work this became possible by the introduction of an explicitly isotropic material discretization in the TMM and the use of a carefully chosen symmetry of the unit cell to avoid the occurrence of cross-polarization scattering amplitudes.[36] In the presence of cross-polarization terms the second polarization can contribute[20] to the T and R of the considered polarization, e.g., the transmission $t_{22} \sim 1$ for the passive polarization of the SRR which has the magnetic field in-plane and the electric field parallel to the gapless sides can cut off the transmission in the active polarization of the SRR in the stop bands, $t_{11}(N) \sim t_{11}^N + t_{12} t_{22}^{N-2} t_{21} + \cdots$, which should decay exponentially with the system length. This effect can cause a phony length dependence in the HEM approximation which is diagonal in the polarizations.

Another issue we have to address is the vacuum wavelength to unit cell size ratio. In the present paper we have 1 (unit cell), 5 (SRR), 25 (low frequency SRR); a typical value for the metamaterials found in the literature is ≈ 10 or worse. Strictly speaking we can expect effective medium behavior only in the $\omega \to 0$ limit. As an approximation, it may hold if the wavelength inside the structure is large compared with the typical length scale of the metamaterial provided by the size of the unit cell. Two points are important here: The relevant wavelength is the wavelength inside the structure and can be much smaller than the corresponding vacuum wavelength if we approach the resonances at ω_m and ω_e and the magnitude of the real part of the effective index of refraction becomes large. Second, we cannot know *a priori* how large the above ratio has to be to reach a reasonable effective medium behavior. Our simulations support both points as the deviations from the expected behavior happen essentially when the wave vector inside the structure $q = n(\omega)k$ becomes comparable with the edge of the Brillouin zone, i.e., the wavelength comparable to the unit cell size; for the low-frequency SRR we find pretty good effective medium behavior without the aforementioned anomalies apart from a small region around the resonance. The simulations indicate that to obtain a reasonable effective medium behavior the wavelength to unit cell size ratio has to be of the order of 30. The less losses occur in the resonances the larger the peak in n, and consequently the required wavelength to unit cell size ratio will be.

Continuum PEM model. The analytic HEM approximation of the periodic medium model proves that the observed deviations from the anticipated effective medium behavior in the HEM approximation of the real simulated metamaterials can be caused by the periodicity or, more precisely, the reduced translational symmetry to the discrete group generated by the unit cell. In particular, the model shows that those artifacts are not related to the actual geometric definition of the SRR and LHM resonances since the homogeneous core in the model just uses the resonant forms of $\mu(\omega)$ and $\varepsilon(\omega)$ without any reference to their microscopic source.

The artifacts observed in the HEM approximation ultimately originate from the occurrence of band gaps introduced by the periodicity, analogously to, for instance, the band structure in a crystal. In our case, the only substantial difference is the explicit frequency dependence of the microscopic material properties, i.e., the resonant forms of $\mu(\omega)$ and $\varepsilon(\omega)$ for the homogeneous core of the periodic medium model's unit cell. These periodicity band gaps are distinct from the intrinsic band gaps which arise directly from the negative product $\varepsilon\mu$ in the emulated response of the constituents. To illustrate the behavior in the periodicity band gaps we assume for the moment $\mu(\omega)$ and $\varepsilon(\omega)$ of the core to be real. Then $n(\omega)$ and $z(\omega)$ in Eq. (23) are simultaneously either real or imaginary and consequently the right-hand side (RHS) of Eq. (23) is real as well. A periodicity band gap occurs whenever the RHS grows outside the domain $[-1,1]$ of the cosine for a real argument: For the principal branch,[45] n_{eff} acquires a nonzero imaginary part inside the gap and $\operatorname{Re} n_{\text{eff}}(\omega)$ retains the value of zero or $\pi/(kL)$ for all RHS of Eq. (23) above 1 or below -1, respectively. Adding a small imaginary part in $\mu(\omega)$ and $\varepsilon(\omega)$ of the core, as should be a good approximation for the emulated metamaterial if we do not come too close to the resonances (absorption peaks), adds a small imaginary part to $n_{\text{eff}}(\omega)$ and causes $\operatorname{Re} n_{\text{eff}}(\omega)$ to deviate slightly from 0 or $\pi/(kL)$ towards $\pi/(2kL)$ inside the periodicity band gap. Having thus established the confinement of the effective index of refraction, $\operatorname{Re} n_{\text{eff}}(\omega)$, to the edge(s) of the fist Brillouin zone or to zero, the coupling of μ and ε follows as a direct consequence.[23] In simple words: If $n^2 = \varepsilon\mu$ is confined and either one of ε,μ exposes resonant behavior the other has to go to zero simultaneously. This also explains why the resonance-antiresonance coupling and the negative imaginary parts occur only across the periodicity band gaps associated with the resonances but not outside. For the general case this qualitative behavior is complicated by the nonzero imaginary parts.

Note again that we can obtain the real part of the index of refraction only as a residue class $\operatorname{Re} n_{\text{eff}}(\omega) \bmod 2\pi/(kL)$ which becomes immediately clear either from the length independence of the HEM approximation of the PEM according to Eqs. (19) and (20) or from the argument about the simultaneous congruences for different system lengths discussed in Sec. II. Therefore the pieces of $\operatorname{Re} n_{\text{HEM}}(\omega)$ that follow the multiples of the first Brillouin zone's edge just coincide with either zero or the first Brillouin zone's edge (upper and lower are equivalent) itself.

Another important observation is that a periodicity band gap may occur in between the magnetic resonance ω_m and the cut-wire resonance ω_e. Unfortunately, the corresponding effective ε looks similar to an electric resonance with the attendant antiresonant structure in μ. This may easily be mistaken as the cut-wire resonance which would be expected to follow the magnetic resonance as the next feature in the frequency spectrum. Only in the low-frequency limit the latter behavior is actually observed. Note that the parameter dependence of the phony electric resonance frequency at the lower edge of the periodicity band gap will qualitatively resemble the behavior of the real cut-wire resonance frequency ω_e.

In comparison to the TMM simulations we see, however, too much structure, i.e., a series of periodicity band gaps instead of only one, around the intrinsic resonances. The ba-

sic difference between the TMM simulation and the analytic calculation of the scattering amplitudes in the continuum is the presence of a finite discretization mesh in the TMM, which implies a smallest distance, hence in turn a largest supported momentum. Obviously, this limitation will become visible where $n_{\mathrm{eff}}(\omega)$ grows large.

Lattice PEM approximation. In our TMM simulations the lattice version of the PEM does better correspond to the numerical data than the continuum PEM. This does also apply to independent Microwave Studio simulations which, in contrast to our TMM simulations, utilize a nonuniform discretization of the metamaterial. If the discretization mesh is chosen finer the lattice PEM gradually approached the continuum PEM behavior.

As discussed above the HEM and the PEM approximation of the real metamaterial are basically length independent, longer systems expose the same spectral features as the first unit cell. However, systems that consist of more than a single unit cell in propagation direction do contribute *additional* tiny resonancelike structures in the effective material constants $\mu_{\mathrm{HEM}}(\omega),\varepsilon_{\mathrm{HEM}}(\omega)$ which are also present in the effective parameters of the PEM approximation $\mu_{\mathrm{PEM}}(\omega)$ and $\varepsilon_{\mathrm{PEM}}(\omega)$ (not shown). For a slab of N unit cells in propagation direction these additional structures appear as tiny band gaps, quite similar to the periodicity band gap discussed above, at frequencies where $n_{\mathrm{PEM}}(\omega)\approx m\pi/(NkL)$ with $m \in [-N,N]\subset\mathbb{Z}$, i.e., whenever the effective refractive index derived from the simple unit cell comes close to the multiples of the first Brillouin zone's edge for the whole slab. The additional structures weaken and eventually cease to be visible in the low-frequency limit as can be seen, for instance, for the SRR in Figs. 7 and 8. Note that again the behavior is generic: it appears in our TMM simulations for LHM, SRR, and also cut-wire and continuous wire metamaterials (not shown), it has also been verified in MICROWAVE STUDIO simulations using a different numeric technique. As there is no such length dependence in the analytic periodic medium model, we interpret this additional "noise" as a limitation of the PEM approximation of the real metamaterial which starts to see some internal structure apart from the explicit periodicity. It is not yet clear whether the groups of N peaks directly at the magnetic resonance are related to this problem. For these there are at least two other interpretations: They may be caused by the coupling of successive SRRs in propagation direction which would lead to the splitting of the resonance frequency ω_m as for the eigenfrequency of coupled identical oscillators, or the finite accuracy of the numeric simulation data could, in particular around the resonances, lead to a residual explicit length dependence.

We demonstrate above that the PEM approximation of real LHM and SRR metamaterials is good in the region around ω_m if the corresponding vacuum wavelength in as small as five times the size of the unit cell. Then we obtained the anticipated effective behavior in $\mu_{\mathrm{HEM}}(\omega),\varepsilon_{\mathrm{HEM}}(\omega)$ and all the anomalies and additional features seen in the HEM approximation arose from the explicit periodicity. If we move to even higher frequency where the vacuum wavelength is close to the size of the unit cell, also $\mu_{\mathrm{HEM}}(\omega)$ and $\varepsilon_{\mathrm{HEM}}(\omega)$ start to develop unexpected features such as additional magnetic response around the cut-wire resonance. Although even then the PEM spectrum is not nearly as erratic as the corresponding HEM spectrum, this indicates the breakdown of the PEM approximation. This is not surprising since we now reach the photonic crystal limit and the internal structure of the metamaterial's constituents must become visible and no "effective description" should be possible anymore.

Physical significance of $\mu_{\mathrm{HEM}}(\omega)$ *and* $\varepsilon_{\mathrm{HEM}}(\omega)$. Although complicated by the periodicity artifacts, such functions are useful to describe the scattering behavior of the metamaterial and allow to make prediction how to design and tune their constituents such as the SRR or the continuous wires. They help to interpret and understand the scattering spectra obtained from experiments and simulations. Last but not least they establish the connection between the low frequency limit where the plain homogeneous medium picture applies with the periodicity artifacts going to zero and the photonic crystal limit which is dominated entirely by the periodicity band structure. All practical realizations of SRR+wire type metamaterials seem to reside within this transition region.

Momentum-dependent parameters. In order to take into account the periodic structure of real metamaterials, we considered the PEM model as a very simple explicit example of a periodic medium. Instead of qualifying the specific geometry of the model used, we may alternatively introduce k-dependent effective parameters $\mu(k,\omega)$, $\varepsilon(k,\omega)$ to describe the spatial distribution of the electromagnetic response in the PEM. These k-dependent effective parameters completely characterize the effective medium model. For the PEM model defined in Fig. 1 we find by Fourier transformation $\varepsilon(k,\omega)=(2\pi)^{-1/2}\int dz\, \varepsilon(z,\omega)e^{ikz}$ the representation

$$\varepsilon(k,\omega) = \sqrt{2\pi}\varepsilon_{\mathrm{core}}(\omega)\frac{e^{ik(L-b)} - e^{ika}}{ikL}\sum_{m\in\mathbb{Z}}\delta\left(k - \frac{2\pi m}{L}\right), \tag{53}$$

and correspondingly for $\mu(k,\omega)$. As a generalization of the periodic medium approximation we could further ask, which arbitrary k dependence of $\varepsilon(k,\omega)$ and $\mu(k,\omega)$, i.e., which spatial distribution of the effective material parameters, describes a given metamaterial best. Although this might be desirable as a descriptive tool for the engineering of metamaterials, it is clearly beyond the scope of this paper.

What is the actual left-handed band? Finally we want to comment on the actual extent of the left-handed interval of the LHM as it concerns experiments and applications. Obviously, the bands with $\mathrm{Re}\, n_{\mathrm{eff}}<0$ retrieved via HEM and PEM approximation differ considerably in width (Fig. 9) which raises the question, where to expect the left-handed behavior. We argue, that the correct region is given by the HEM approximation. If there is a length-independent HEM approximation, the scattering behavior of the metamaterial can be described assuming plain-wave solutions inside the homogeneous unit cell. These plain waves will possess a wave-vector q related to the vacuum-wave-vector k by the retrieved negative index of refraction $q=n_{\mathrm{HEM}}(\omega)k$. They coincide with the nonperiodic factor of the Bloch waves describing the periodic medium, i.e., coincide with the Bloch

waves at the edges of the unit cells in the metamaterial. Therefore a (usually damped) plain wave with negative phase velocity will exist inside the metamaterial whenever $\mathrm{Re}\, n_{\mathrm{HEM}} < 0$. This interpretation is also supported by experimental measurements.[9] Note that this frequency interval is wider than the interval with simultaneously negative $\mathrm{Re}\, \varepsilon_{\mathrm{HEM}}$ and $\mathrm{Re}\, \mu_{\mathrm{HEM}}$. The PEM approximation indicates that the isolated local response of the SRR and wire, without the effects of periodicity, would lead to a much smaller left-handed band (compare the behavior of the low-frequency SRR, Figs. 7 and 8). The modifications of the generic response of SRR and wire by the band structure, in particular by the emergence of periodicity band gaps, arising from the inherent periodicity of the metamaterial, greatly enhances the width of the negative index band in metamaterials which see strong artifacts from the periodicity. This concerns virtually all published metamaterials with a vacuum wavelength to unit cell length ratio smaller than approximately ten. At much lower frequency, truly effective homogeneous behavior will emerge, the periodicity band gaps disappear, and HEM and PEM description coincide.

Geometry of the PEM model. As we demonstrated in Sec. III, for the quasi one-dimensional scattering problem of a system comprised of an integral number of unit cells in propagation direction, we can exactly describe any HEM by a family of PEM, parametrized by the geometry $\mathcal{G}=(n_a, n_d, n_b)$ of the periodic medium model (see Fig. 1), in terms of effective parameters $\mu_{\mathrm{PEM}[\mathcal{G}]}(\omega)$ and $\varepsilon_{\mathrm{PEM}[\mathcal{G}]}(\omega)$. For a simulated metamaterial, in general all effective parameters, $\mu_{\mathrm{HEM}}(\omega)$ and $\varepsilon_{\mathrm{HEM}}(\omega)$ as well as $\mu_{\mathrm{PEM}[\mathcal{G}]}(\omega)$ and $\varepsilon_{\mathrm{PEM}[\mathcal{G}]}(\omega)$, will show "unphysical" behavior caused by the internal spatial structure of the unit cell and the periodicity of the metamaterials. If for a real metamaterial the local electromagnetic behavior of the constituents can be abstracted from their geometrical form, approximated by simple resonant and plasmonic response functions $\mu_{\mathrm{SRR}}(\omega)$ and $\varepsilon_{\mathrm{wire}}(\omega)$, respectively, and separated from the effects of the periodicity (i.e., band structure), then there is a particular geometry of the PEM which approximates physical parameters $\mu_{\mathrm{PEM}[\mathcal{G}]} \times(\omega) \approx \mu_{\mathrm{SRR}}(\omega)$ and $\varepsilon_{\mathrm{PEM}[\mathcal{G}]}(\omega) \approx \varepsilon_{\mathrm{wire}}(\omega)$ without the usual artifacts discussed in this paper. In our simulations the best such approximation was obtained if the lattice PEM containing a single plain of scatterers in the unit cell, i.e., for a geometry $\mathcal{G}=(5,1,4)$.

VI. CONCLUSION

We have investigated the influence of the inherent periodic structure always present in metamaterials which are built from the repetition of a single unit cell on the effective medium approximation. It has been shown analytically that all the previously observed violations of the anticipated effective medium behavior of the (single-ring) SRR and LHM involving a single magnetic and a single electric resonance can be explained in terms of the periodic structure: A very simple stratified periodic medium model involving slabs of vacuum alternating with slabs of a homogeneous material with simple resonant $\mu(\omega)$ and $\varepsilon(\omega)$ can reproduce all the artifacts such as resonance-antiresonance coupling in $\mu_{\mathrm{HEM}}(\omega)$ and $\varepsilon_{\mathrm{HEM}}(\omega)$, negative imaginary parts in either ε or μ, truncated, misshapen resonances, additional band gaps and the complicated high-frequency behavior found in the HEM approximation of numerically simulated SRR arrays and LHM, but also metamaterials built of continuous wires and of cut wires. In good approximation, the effective behavior can be decomposed into an effective behavior of the constituents of the metamaterial and an explicit contribution of the periodicity. Remarkably, the average contribution of constituents such as the single split-ring behaves much as expected from the assumed homogeneous medium picture, which can only be justified in the low-frequency limit where the wavelength inside the structure is large compared to its geometrical size, up to frequencies where the vacuum wave length becomes comparable to the size of the unit cell. This allows a more reliable effective description and interpretation of real metamaterials in terms of a periodic effective medium (PEM) instead of the conventional homogeneous effective medium (HEM) with all the hard to understand artifacts. The effects caused by the periodicity are generic, they do qualitatively not depend on the particular geometry chosen for the metamaterial and universally apply to SRR, LHM, continuous wire and cut-wire materials. Obviously, the impact of the periodicity is noticeable throughout the range of the λ_0/L ratio $\approx 5 \cdots 10$ (i.e., vacuum wave length/unit cell length) actually found in published simulations and experiments for left-handed and related metamaterials. Our simulations indicate that an unencumbered homogeneous effective medium behavior, though reachable in the low-frequency limit, would require a λ_0/L ratio in the order of 30 or larger which is geometrically not easy to obtain in real samples. We investigated the difference between the continuum and the lattice formulation of the PEM approximation and found the latter to be better suited for application to our numerically simulated scattering data for real metamaterials obtained with a lattice-TMM implementation.

The PEM approximation may provide a valuable tool to understand the various features observed in the scattering spectra of real metamaterials in experiments and simulations. In the present paper we essentially discussed the vicinity of the magnetic resonance of the SRR. Further work shall emphasize on the frequencies above the magnetic resonance ω_m including the cut-wire resonance ω_e.

We expect the impact of the metamaterial's periodicity to be noticeable also in higher dimensional structures. Because the unit cells of those structures tend to be more complicated including couplings of SRRs in the different directions the separation of the "real" effective response of the constituents and the structures produced by the periodicity constitutes an even more imminent issue for understanding.

ACKNOWLEDGMENTS

This work was partially supported by Ames Laboratory (Contract No. W-7405-Eng-82). Financial support of EU_FET project DALHM, NATO (Grant No. CBP.EAP-.CLG.981471), and DARPA (Contract No. MDA972-01-2-0016) are also acknowledged. P.M. thanks APVT (Grant No. 51-021602) for partial financial support.

[1] V. G. Veselago, Usp. Fiz. Nauk **92**, 517 (1967) [Sov. Phys. Usp. **10**, 509 (1968)].
[2] J. B. Pendry, A. J. Holden, W. J. Stewart, and I. Youngs, Phys. Rev. Lett. **76**, 4773 (1996).
[3] J. B. Pendry, A. J. Holden, D. J. Robbins, and W. J. Stewart, J. Phys.: Condens. Matter **10**, 4785 (1998).
[4] J. B. Pendry, A. J. Holden, D. J. Robbins, and W. J. Stewart, IEEE Trans. Microwave Theory Tech. **47**, 2057 (1999).
[5] D. R. Smith, W. J. Padilla, D. C. Vier, S. C. Nemat-Nasser, and S. Schultz, Phys. Rev. Lett. **84**, 4184 (2000).
[6] R. A. Shelby, D. R. Smith, S. C. Nemat-Nasser, and S. Schultz, Appl. Phys. Lett. **78**, 489 (2001).
[7] R. A. Shelby, D. R. Smith, and S. Schultz, Science **292**, 77 (2001).
[8] D. R. Smith and N. Kroll, Phys. Rev. Lett. **85**, 2933 (2000).
[9] C. G. Parazzoli, R. Greegor, K. Li, B. E. C. Koltenbach, and M. Tanielian, Phys. Rev. Lett. **90**, 107401 (2003).
[10] A. A. Houck, J. B. Brock, and I. L. Chuang, Phys. Rev. Lett. **90**, 137401 (2003).
[11] P. Markoš and C. M. Soukoulis, Phys. Rev. B **65**, 033401 (2002).
[12] P. Markoš and C. M. Soukoulis, Phys. Rev. E **65**, 036622 (2002).
[13] P. Markoš, I. Rousochatzakis, and C. M. Soukoulis, Phys. Rev. E **66**, 045601(R) (2002).
[14] D. R. Smith, S. Schultz, P. Markoš, and C. M. Soukoulis, Phys. Rev. B **65**, 195104 (2002).
[15] M. M. Sigalas, C. T. Chan, K. M. Ho, and C. M. Soukoulis, Phys. Rev. B **52**, 11 744 (1995).
[16] A. K. Sarychev and V. M. Shalaev, cond-mat/0103145 (unpublished).
[17] A. L. Pokrovsky and A. L. Efros, Phys. Rev. Lett. **89**, 093901 (2002).
[18] T. Weiland, R. Schummann, R. B. Greegor, C. G. Parazzoli, A. M. Vetter, D. R. Smith, D. V. Vier, and S. Schultz, J. Appl. Phys. **90**, 5419 (2001).
[19] S. O'Brien and J. B. Pendry, J. Phys.: Condens. Matter **14**, 6383 (2002); **14**, 4035 (2002).
[20] P. Markoš and C. M. Soukoulis, Opt. Express **11**, 649 (2003).
[21] X. Chen, T. M. Grzegorczyk, B-I. Wu, J. Pacheco, Jr., and J. A. Kong, Phys. Rev. E **70**, 016608 (2004).
[22] S. O'Brien, D. McPeake, S. A. Ramakrishna, and J. B. Pendry, Phys. Rev. B **69**, 241101(R) (2004).
[23] T. Koschny, P. Markoš, D. R. Smith, and C. M. Soukoulis, Phys. Rev. E **68**, 065602(R) (2003).
[24] R. A. Depine and A. Lakhtakia, Phys. Rev. E **70**, 048601 (2004).
[25] A. L. Efros, Phys. Rev. E **70**, 048602 (2004).
[26] T. Koschny, P. Markoš, D. R. Smith, and C. M. Soukoulis, Phys. Rev. E **70**, 048603 (2004).
[27] A. L. Efros and A. L. Pokrovsky, Solid State Commun. **129**, 643 (2004).
[28] T. J. Yen, W. J. Padilla, N. Fang, D. C. Vier, D. R. Smith, J. B. Pendry, D. N. Basov, and X. Zhang, Science **303**, 1494 (2004).
[29] T. Koschny, M. Kafesaki, E. N. Economou, and C. M. Soukoulis, Phys. Rev. Lett. **93**, 107402 (2004).
[30] M. Born and E. Wolf, *Principles of Optics* (MacMillan, New York, 1964).
[31] J. B. Pendry and A. MacKinnon, Phys. Rev. Lett. **69**, 2772 (1992).
[32] J. B. Pendry, A. MacKinnon, and P. J. Roberts, Proc. R. Soc. London, Ser. A **437**, 67 (1992).
[33] J. B. Pendry, J. Mod. Opt. **41**, 209 (1994).
[34] J. B. Pendry and P. M. Bell, in *Photonic Band Gap Materials*, Vol. 315 of *NATO Advanced Studies Institute, Ser. E: Appl. Sci.*, edited by C. M. Soukoulis (Plenum, New York, 1996), p. 203.
[35] N. Katsarakis, T. Koschny, M. Kafesaki, E. N. Economou, and C. M. Soukoulis, Appl. Phys. Lett. **84**, 2943 (2004).
[36] T. Koschny *et al.* (unpublished).
[37] K. Li, S. J. McLean, R. B. Greegor, C. G. Parazzoli, and M. Tanielian, Appl. Phys. Lett. **82**, 2535 (2003).
[38] E. Ozbay, K. Aydin, E. Cubukcu, and M. Bayindir, IEEE Trans. Antennas Propag. **51**, 2592 (2003).
[39] M. Bayindir, K. Aydin, E. Ozbay, P. Markoš, and C. M. Soukoulis, Appl. Phys. Lett. **81**, 120 (2002).
[40] N. Katsarakis, T. Koschny, M. Kafesaki, E. N. Economou, E. Ozbay, and C. M. Soukoulis Phys. Rev. B **70**, 201101(R) (2004).
[41] N. Katsarakis (private communication).
[42] R. Marqués, F. Medina, and R. Rafii-El-Idrissi, Phys. Rev. B **65**, 144440 (2002).
[43] S. Bassiri, C. H. Papas, and N. Engheta, J. Opt. Soc. Am. A **5**, 1450 (1988).
[44] We consider the transfer matrix $\mathbb{T}$ for a planar stratified medium in the z direction. Because $\mathrm{div}\,\mathbf{D}=0$, $\mathrm{div}\,\mathbf{B}=0$, the source-free Maxwell equations only allow for four independent field components $\mathbb{F}=(E_x,E_y,H_x,H_y)$, $\mathbb{F}(z+dz)=\mathbb{T}(z)\mathbb{F}(z)$. The eigensystem $\{k,\mathbb{F}_k\}$ of the transfer matrix inside the strata, $\mathbb{T}(z)\mathbb{F}_k(z)=e^{ik\,dz}\mathbb{F}_k(z)$, defines the plain wave base (including propagating and evanescent waves) for the scattering problem. Local z isotropy implies that with each k also $-k$ is eigenvalue such that the wave basis splits into right- and left-going waves, while translational invariance of the stratified medium $\perp z$ factorizes the transfer matrix with respect to the momentum $k_\parallel$ parallel to the strata which is preserved across interfaces. Within a $(|k|,k_\parallel)$ subspace the E and H fields are dependent, coupled by the Maxwell equations, such that we can decompose $\mathbb{F}$ as a linear combination of only two polarizations, e.g., TE and TM mode. For the TE mode, the electric field $\mathbf{E}$ is parallel to the interface and we can express it inside each stratum as a linear combination $(Ae^{ikz}+Be^{-ikz})e^{ik_\parallel r_\parallel}$. For the TM mode the same applies to the magnetic field $\mathbf{H}$. In either case we can write a transfer matrix for the wave amplitudes across a single interface as $(A'B')^T=\mathcal{T}_{kk'}(z)(AB)^T$, where $\mathcal{T}_{kk'}(z)=\phi_{k'}^{-1}(z)T_{kk'}\phi_k(z)$ can be written as product over phase factors ϕ and the location independent matrix $T_{kk'}$ which coincides with the transfer matrix for the fields $(\psi_k\ \psi_{-k})=(Ae^{ikz}\ Be^{-ikz})$ instead of the amplitudes. In explicit form we have

$$\phi_k(z)=\begin{pmatrix} e^{ikz} & 0 \\ 0 & e^{-ikz}\end{pmatrix},\quad T_{kk'}=\frac{1}{2}\begin{pmatrix} 1+\zeta_{kk'} & 1-\zeta_{kk'} \\ 1-\zeta_{kk'} & 1+\zeta_{kk'}\end{pmatrix},$$

with $\zeta_{kk'}=\mu' k/(\mu k')$ for the TE and $\varepsilon' k/(\varepsilon k')$ for the TM mode. The transfer matrix for a vacuum-terminated stack of N layers has the composition property $T_{13}=T_{23}T_{12}$ and inserting a virtual vacuum interface $T_{k_n k_{n+1}}=T_{k_{\mathrm{vac}}k_{n+1}}T_{k_n k_{\mathrm{vac}}}$ between each adjacent two layers we get an expression

$$\mathcal{T}_{\mathrm{total}}(k_{\mathrm{vac}})=\phi_{\mathrm{vac}}^{-1}(z_N)\left[\prod_{n=1}^{N}T_{\mathrm{slab}}(z_n-z_{n-1})\right]\phi_{\mathrm{vac}}(z_0)$$

with the interfaces located at z_n and the local transfer matrix of a single layer $T_{\mathrm{slab}}(d)=T_{k_n k_{\mathrm{vac}}}\phi_{k_n}(d)T_{k_{\mathrm{vac}}k_n}$ which is given explicitly in Sec. II.

[45] We define the principal branch of $\arg(z)$ as $-\pi < \arg z \leqslant \pi$ with a branch cut along the negative real axis, continuous from the second quadrant. Then the principal branches of $\sqrt{z} = |z|^{1/2} \exp[i \arg(z)/2]$ and $\ln(z) = \ln|z| + i \arg(z)$ can be defined with the same branch cut and continuity from above. Using $2\cos(z) = \exp(iz) + \exp(-iz)$ we obtain the principal branch $\arccos(z) = -i \ln(z + i\sqrt{1-z^2})$ with a branch cut on the real axis for $z \in (1, \infty)$, continuous from below, and $z \in (-\infty, -1)$, continuous from above.